AD-A127 139 EVALUATION OF AURORA AS A TACTICAL SOURCE REGION SIMULATION(U) MISSION RESEARCH CORP SANTA BARBARA CA W F CREVIER ET AL. FEB 83 AURORA-EMP-MEMO-21 1/1

UNCLASSIFIED HDL-CR-83-072-2 DAAK21-80-R-9072 F/G 14/2 NL

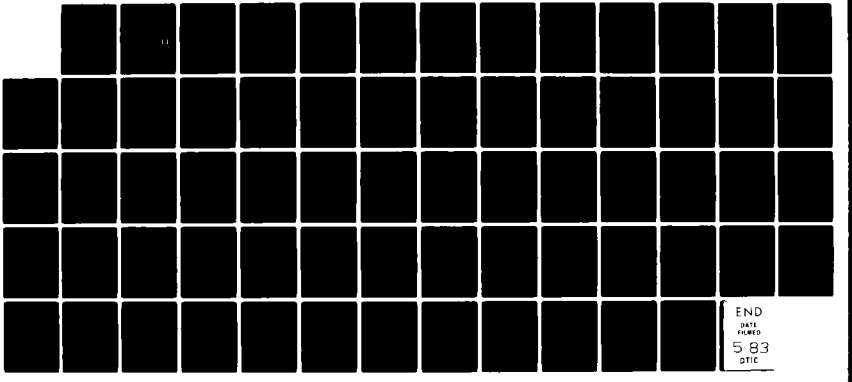

END
DATE FILMED
5 83
DTIC

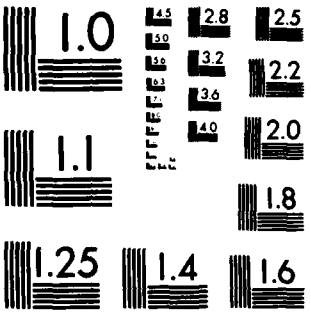

(12)

AD A127 139

HDL-CR-83-072-2

February 1983

Evaluation of AURORA as a Tactical Source Region Simulation

by W. F. Crevier
E. D. Kalasky

Prepared by

Mission Research Corporation
735 State Street
Post Office Drawer 719
Santa Barbara, CA 93102

Under contract

DAAK21-80-R-9072

U.S. Army Electronics Research and Development Command
Harry Diamond Laboratories
Adelphi, MD 20783

DTIC FILE COPY

The findings in this report are not to be construed as an official Department of the Army position unless so designated by other authorized documents

Citation of manufacturers' or trade names does not constitute an official indorsement or approval of the use thereof

Destroy this report when it is no longer needed. Do not return it to the originator

UNCLASSIFIED

SECURITY CLASSIFICATION OF THIS PAGE (When Data Entered)

REPORT DOCUMENTATION PAGE		READ INSTRUCTIONS BEFORE COMPLETING FORM
1. REPORT NUMBER HDL-CR-83-072-2	2. GOVT ACCESSION NO. AD-A127139	3. RECIPIENT'S CATALOG NUMBER
4. TITLE (and Subtitle) Evaluation of AURORA as a Tactical Source Region Simulation		5. TYPE OF REPORT & PERIOD COVERED Contractor Report 6. PERFORMING ORG. REPORT NUMBER AURORA EMP Memo-21
7. AUTHOR(s) W. F. Crevier E. D. Kalasky HDL Contact: William Scharf		8. CONTRACT OR GRANT NUMBER(s) DAAK21-80-R-9072
9. PERFORMING ORGANIZATION NAME AND ADDRESS Mission Research Corporation 735 State Street Santa Barbara, CA 93102		10. PROGRAM ELEMENT, PROJECT, TASK AREA & WORK UNIT NUMBERS Program Element: 62120A DA Project: 1L162120AH25
11. CONTROLLING OFFICE NAME AND ADDRESS Harry Diamond Laboratories 2800 Powder Mill Road Adelphi, MD 20783		12. REPORT DATE February 1983 13. NUMBER OF PAGES 67
14. MONITORING AGENCY NAME & ADDRESS(if different from Controlling Office)		15. SECURITY CLASS. (of this report) UNCLASSIFIED 15a. DECLASSIFICATION/DOWNGRADING SCHEDULE

16. DISTRIBUTION STATEMENT (of this Report)

Approved for public release; distribution unlimited.

17. DISTRIBUTION STATEMENT (of the abstract entered in Block 20, if different from Report)

18. SUPPLEMENTARY NOTES

HDL Project: X750E7
DRCMS Code: 612120H250011

19. KEY WORDS (Continue on reverse side if necessary and identify by block number)

SREMP	Simulation
AURORA	Radiation
Flash x ray	Nuclear effects

20. ABSTRACT (Continue on reverse side if necessary and identify by block number)

This memo compares the AURORA environment with that expected in an actual tactical source region environment. The primary interest in making the comparison is to evaluate the role that AURORA can play as a source region simulator for tactical systems of interest to the U.S. Army. Comparisons are made between the electric and magnetic fields measured in AURORA and those computed using a four source model of AUR3D. Excellent agreement is found in the comparison between the magnetic fields. The computed electric fields show a fundamentally different behavior from those measured in AURORA.

DD FORM 1 JAN 73 1473 EDITION OF 1 NOV 65 IS OBSOLETE

UNCLASSIFIED

SECURITY CLASSIFICATION OF THIS PAGE (When Data Entered)

CONTENTS

FIGURES

FIGURES (Cont'd)

Page

FIGURES (Cont'd)

TABLES

INTRODUCTION

In this memo we will be concerned with how the environment generated by the Defense Nuclear Agency's AURORA flash x-ray machine compares with that expected in an actual tactical source region environment. Our primary interest in making this comparison is to evaluate the role that AURORA can play as a source region simulator for tactical systems of interest to the U.S. Army. Here we will not discuss IEMP problems where the Compton electrons from AURORA drive the fields inside of a piece of equipment. Instead, our concern will be with the fields generated in the AURORA room itself and how, for example, various antennae might respond to those fields.

There has been some question in the past about the need to modify or enhance the electric fields in AURORA to make them more realistic. We will address this question in detail and make comparisons between the unmodified AURORA environments and a "typical" source region environment. The comparisons will be made with regard to the generation mechanisms as well as with regard to the fields themselves. The fields will be compared in both the frequency and time domain. Since many systems respond primarily to the time-rate-of-change of $\vec{E}$ and $\vec{B}$, we will also make comparisons with these quantities.

THE TACTICAL SOURCE REGION

The term "source region" is used to distinguish the volume around a nuclear burst, which contains the sources of the EMP - γ-rays and neutrons, from the volume beyond it which just contains the electro-magnetic fields that propagate from the source region. The inner edge of the source region is the burst point. The outer edge is not well defined since the sources decay exponentially and theoretically have a finite value everywhere. Various criteria for what constitutes the outer edge of the source region for surface and near surface bursts have been proposed.[1] They are usually based upon comparisons between the displacement currents and conduction current or on a 1/R fall off of the fields with range. Generally the source region is considered to extend 2 or 3 km from a surface or near surface burst. Here we are not really concerned with the outer edge of the source region. Rather, we wish to examine the U.S. Army's criteria for defining the inner edge of the source region for tactical systems - what we call the tactical source region.

Source region environments can generally be divided up into two types - strategic and tactical. The strategic source region is generated by a large yield burst - in the megaton range. Strategic systems are often buried and designed to survive in close to such bursts. The air above them is exposed to dose rates in the 10^{12}-10^{13} rad/sec range. The air conductivity can reach 2 mho/meter or more which is well above typical soil conductivities (10^{-2} to 10^{-3} mho/m).

The tactical source region is generated by lower yield bursts—say below 50 kT. Also tactical systems are usually on or above the ground and so can not survive in very close to a nuclear burst. The inner edge of the tactical source region is determined by the system (or human) vulnerabilities to weapon effects other than EMP, such as blast and shock, thermal radiation, or initial gamma and neutron radiation. The army uses a balanced hardening approach which simply states that if a system and its crew can survive these other nuclear weapon effects it should not fail due to EMP.[2]

Thus, the inner edge of the tactical source region ends up not being defined in terms of maximum E-fields or currents but rather in terms of overpressure or thermal radiation. This makes it difficult to define an EMP environment at the inner edge of the source region since the scaling with yield and range for the EMP sources is different than that for these mechanical effects. This is especially true for exposed personnel where thermal radiation is the dominant effect for yields over 1 kt.

For persons protected from direct thermal radiation, by trucks or signal shelters for example, the inner edge of the source region is determined by early transient incapacitation (ETI) of the crew due to exposure to nuclear radiation from a burst. ETI is a temporary inability to perform a task. Doses in the 2000 to 5000 rad range produce almost immediate incapacitation.[3]

If one uses ETI to define the inner edge of the tactical source region there can be some correlation between the dose level selected as the highest a person can be exposed to and the tactical source region environment since the sources of the two effects are related. Early transient incapacitation is determined by the immediate neutron and γ-radiation that which comes out in the first few seconds. Typically 3 percent of the yield is in such radiation.[3] The EMP is driven by the prompt γ-radiation - that which comes out in a fraction of a μ-second. Typically 0.1 percent of the yield is in prompt γ-radiation. Additional radiation sources continue to generate a significant EMP out to times of a millisecond or more but here we are primarily concerned with the early time peaks where the fields and sources are strongest and changing most rapidly.

The ratio between the immediate and prompt radiation sources can vary considerably as a function of yield and device design. In some cases the EMP at the man survivability range from a small yield burst can be more stressing than that from a larger yield burst. But, in spite of this variability, it is useful to have a specific environment to refer to. Following Reference 4, we take 50 kT yield as the upper limit for weapons of tactical interest and

assume that 3 percent of the yield is in initial neutron and γ-radiation. A typical mean free path (λ) at sea level for such radiation is 3×10^{4} cm. Using the fact that 1 kT equals 4.18×10^{19} ergs; 1 rad = 100 ergs/gm, and $\rho = 1.23\times10^{-3}$ gm/cm^3, we find that the immediate dose at a radius r is

$$D = \frac{Y\times0.03\times4.18\times10^{18}\ e^{-r/\lambda}}{100\times4\pi r^2\rho\lambda}$$

$$D = 1.35\times10^{15}\ e^{-r/\lambda}/r^2 \quad \text{rads}$$

Table 1 shows the immediate dose as a function of range from this hypothetical device. Since doses in the 2000 to 5000 rad range produce almost immediate incapacitation, the inner edge of the tactical source region is limited to somewhere between 1.0 and 1.5 km. Figures 1 through 3 show how the peak values of various parameters of interest vary with range from a 50 kT burst. The results were generated with the Mission Research Corpoation - Harry Diamond Laboratory interactive EMP coupling code MODELC.[5] The code uses

Table 1. Immediate dose as a function of range for 50 kT yields.

RANGE	IMMEDIATE DOSE
0.5 km	102,000 rads
0.8 km	14,700 rads
1.0 km	4,800 rads
1.2 km	1,700 rads
1.5 km	400 rads
2.0 km	40 rads

analytic approximations and 1-D numerical integration algorithms to solve for quantities at the ground-air interface. The MODELC equations assume a perfectly conducting ground. A water vapor content of 1 percent was used for these examples. Only peaks before 1 μsec were considered.

In Figure 1 we have plotted the vertical and radial electric fields along with $-cB_\phi$ for ease of comparison. All quantities have units of volts/meter. To convert cB_ϕ to Amps/meter just divide by the impedance of free space, 377 Ω. Inside about 1500 meters the magnetic field dominates because air conductivity limits the electric fields. Beyond 2000 meters the transverse magnetic and electric fields peak at near their free space ratio which indicates that local air conductivity is not too important, at least for peak values. Note that the propagated fields, B_ϕ and E_θ, do not fall off with range as fast as E_r which is driven by the local sources.

The E_r shown here includes the radial Compton current and conduction current but neglects the curl $\vec{B}$ term. It is the E_r that would exist in the absence of the ground and can be considered as a reasonable upper limit to the radial electric field near the ground.

The peak Compton current and air conductivity graphs (Figures 2 and 3) indicate that there is a much larger variation with range for these quantities. Note that the peak air conductivity between 1000 and 1500 meters is in the 10^{-4} range which is below the conductivity of most soils. The total immediate dose we estimated above has nearly the same radial dependence as the Compton current. Multiplying the current in Figure 2 by 100 gives an estimate of the immediate dose.

For a specific environment we select 1200 m from this 50 kt device as a reasonable inner limit to the tactical source region. The immediate dose is estimated to be 1700 rads at 1200 meters. Figures 4 through 6 show the time history of the magnetic field, the vertical and radial electric fields,

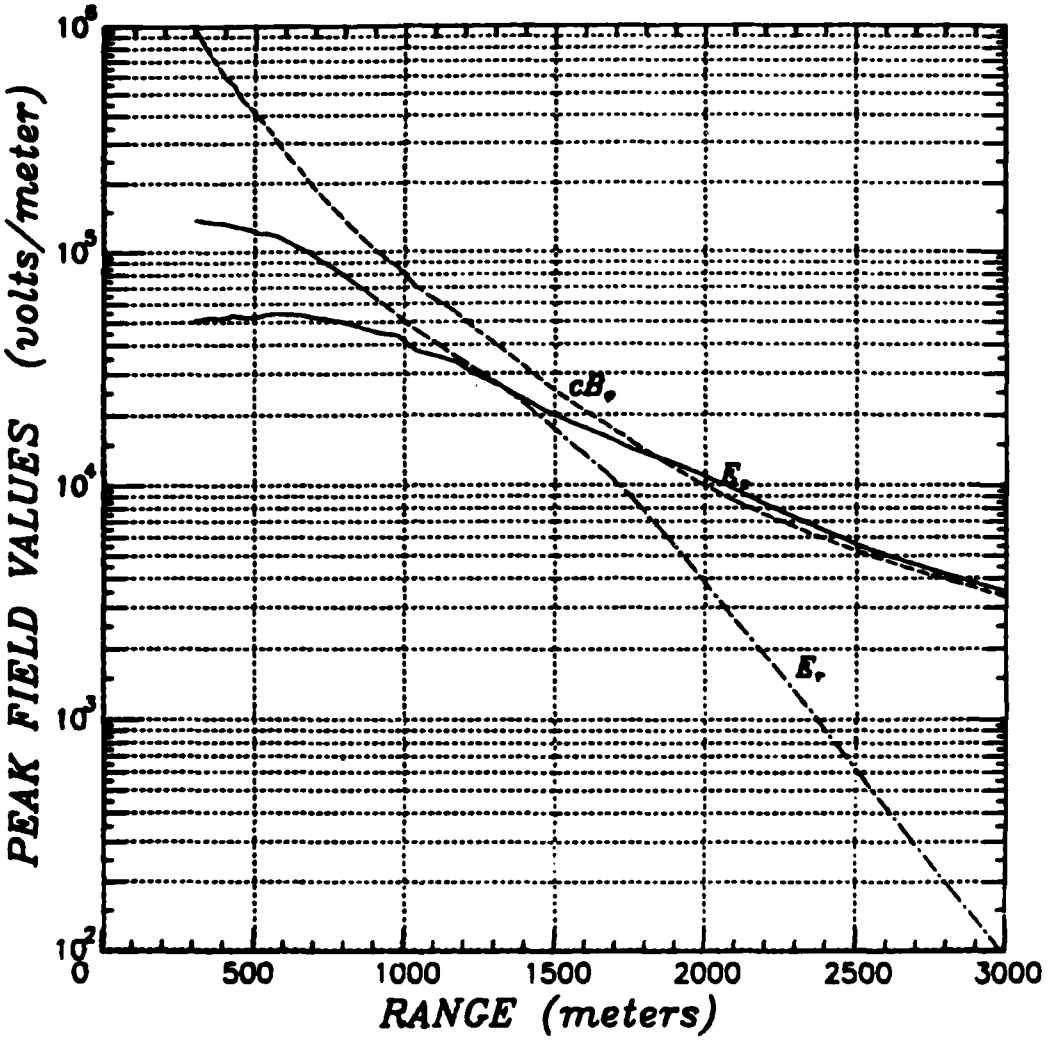

Figure 1. Peak values of E_r, E_z, and $-cB_\phi$ vs range for a 50 kT surface burst.
(Note: $-E_\theta$ at ground level is E_z.)

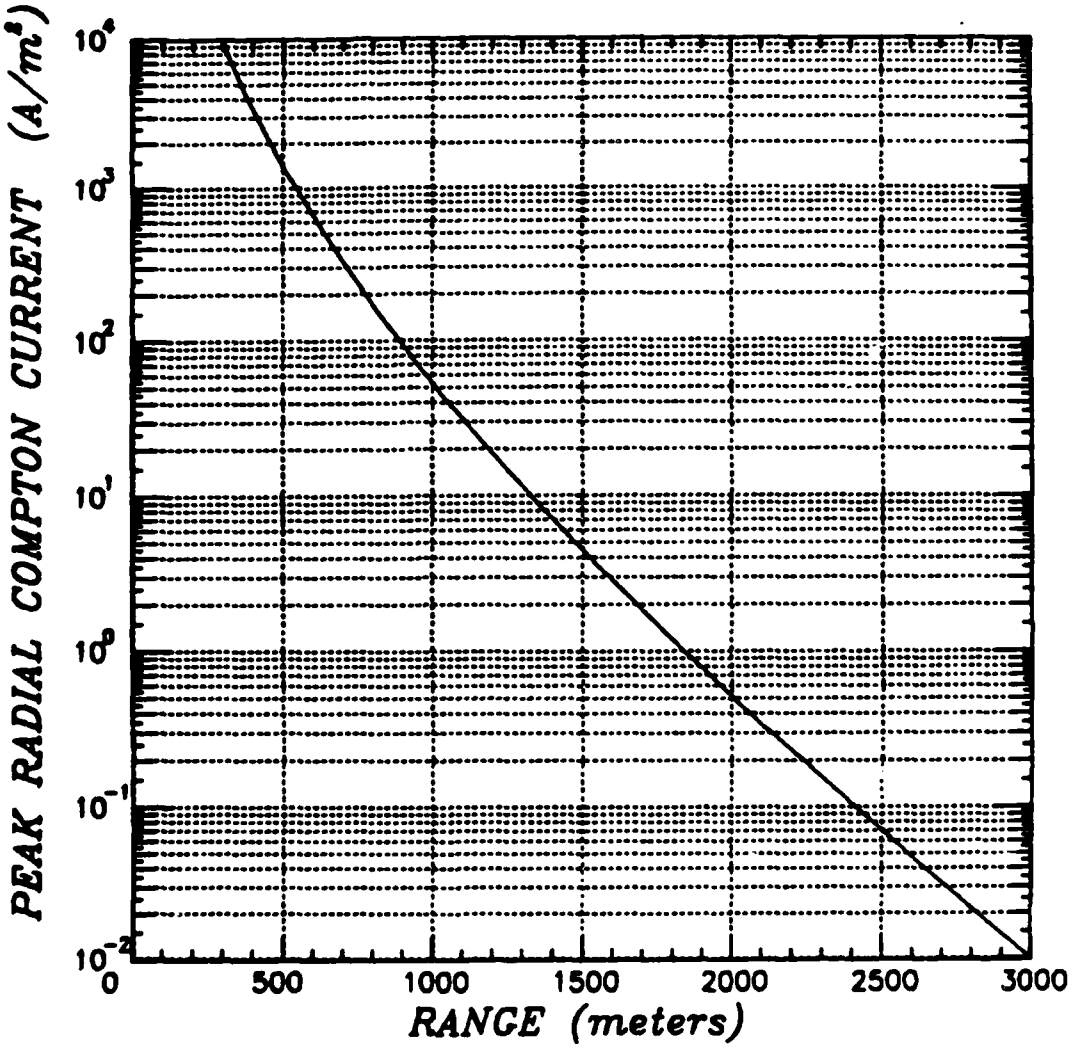

Figure 2. Peak radial Compton current vs range for a 50 kT surface burst. The Compton current is in the negative r-direction.

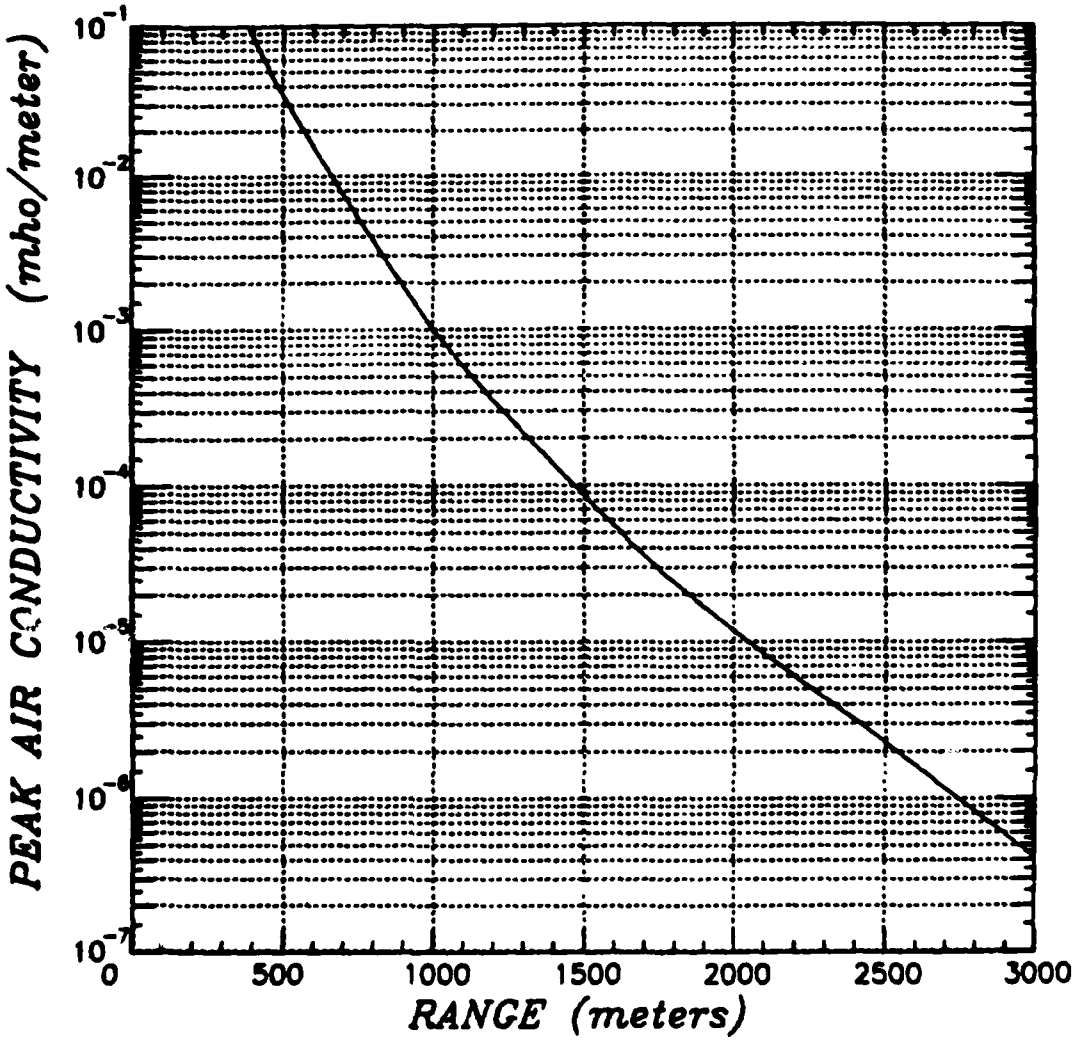

Figure 3. Peak air conductivity vs range for a 50 kT surface burst. A 1 percent water vapor content was assumed.

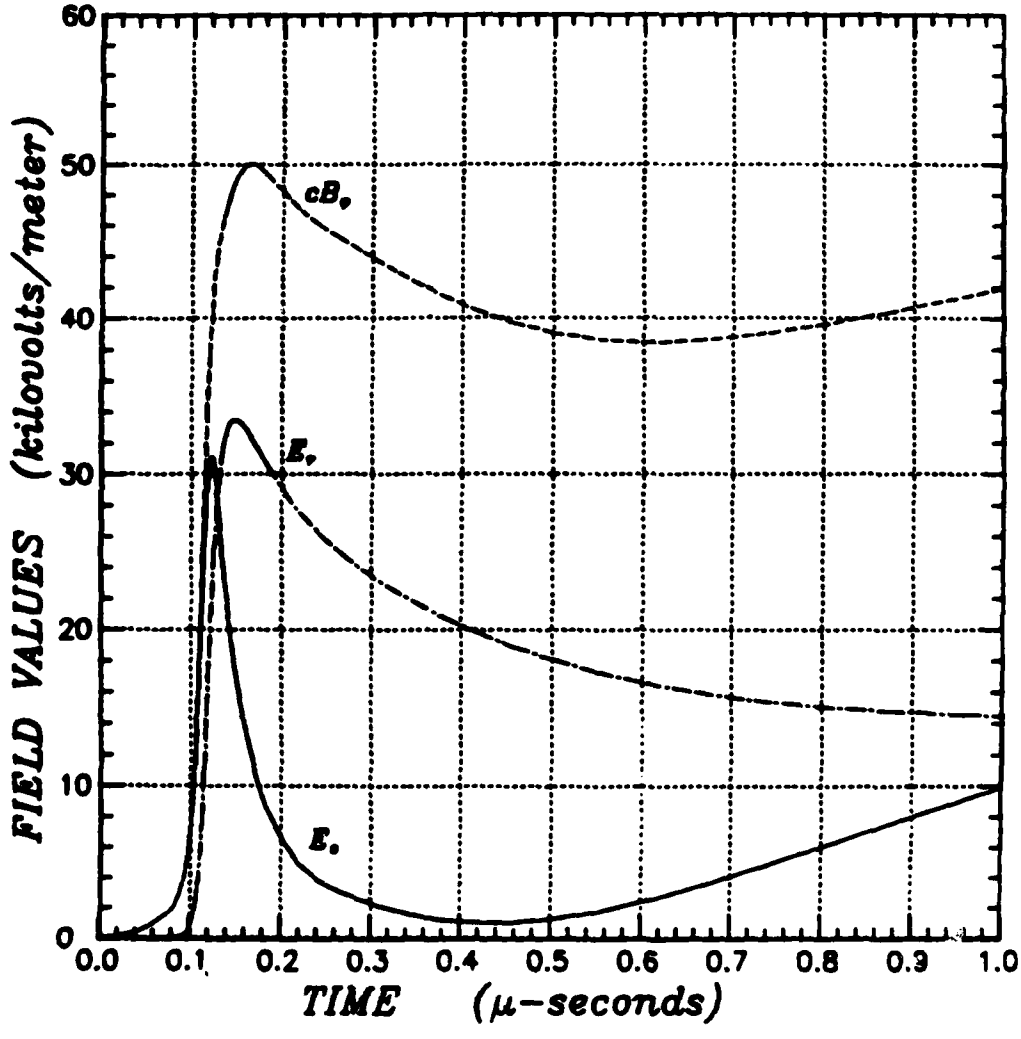

Figure 4. Time histories of $-cB_\phi$, E_r and E_z 1200 m from a 50 kT surface burst. Note that the scale is in kilovolts/meter.

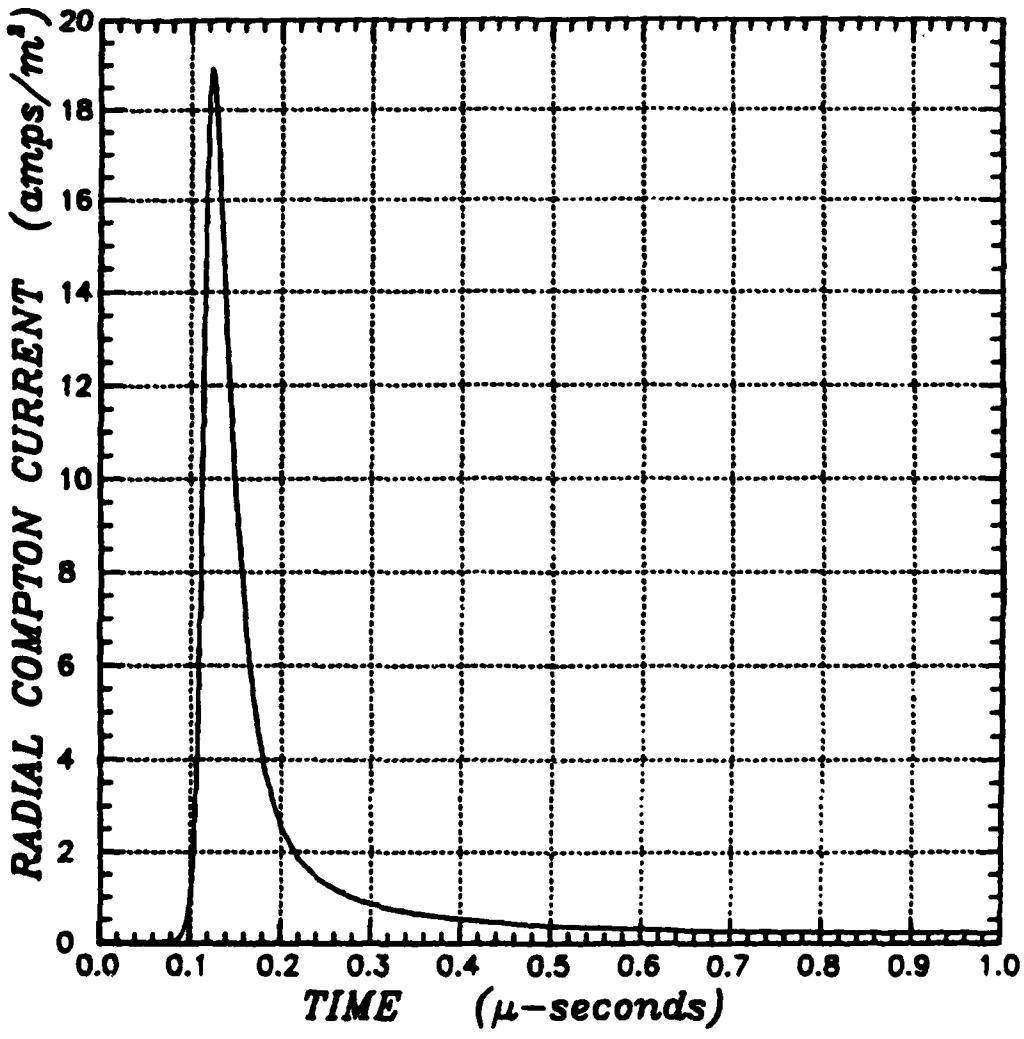

Figure 5. Time history of the magnitude of the radial Compton current 1200 m from a 50 kT surface burst. The radial component of the Compton current is negative.

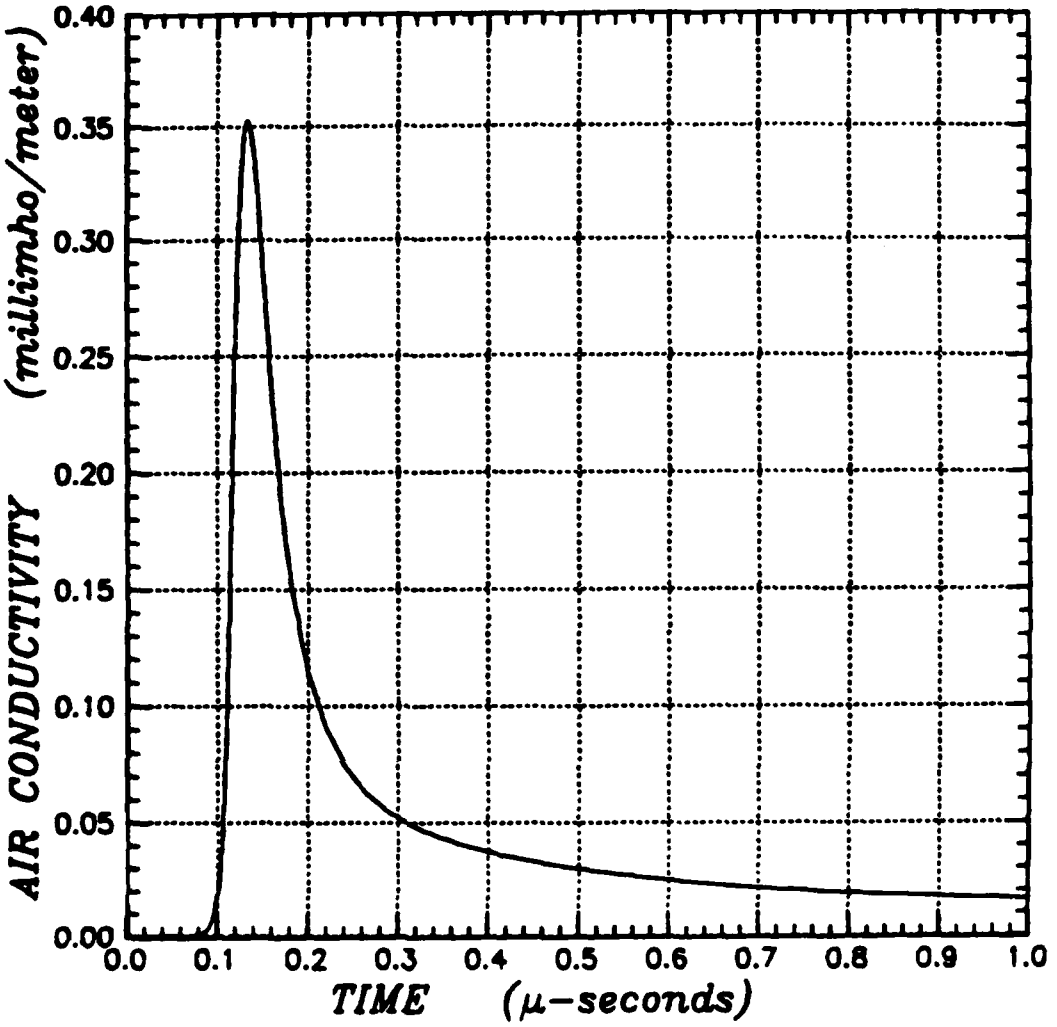

Figure 6. Time history of the air conductivity 1200 m from a 50 kT surface burst. A 1 percent water vapor was assumed. Note that the scale is in millimho/meter.

Compton current, and air conductivity out to 1 μsec. Note that the magnetic field stays high and in fact continues to increase somewhat after the peak in the Compton current at 0.12 μsec. The vertical electric field, on the other hand, peaks at about the same time as the Compton current and then falls to near zero before starting to rise again at late times.

SOURCE REGION EMP GENERATION MECHANISMS

The EMP environment in AURORA and other flash X-ray machines is quite different from that generated by a nuclear explosion. The differences are not just in magnitude, they are fundamental consequences of the differences in geometries. To really understand the shortcomings of EMP simulations one must first understand how the nuclear EMP is generated and how that is different from the EMP generation process in a simulator such as AURORA.

The basic geometry of a surface burst is best treated in spherical coordinates. The polar angle, θ, is measured from the vertical. Because of the azimuthal symmetry only E_r and E_θ* components of the electric field are generated. An azimuthal component of magnetic field, B_ϕ, is also generated. The relevant Maxwell's equations are:

$$\frac{\partial B_\phi}{\partial t} = - \frac{1}{r} \frac{\partial}{\partial r} (rE_\theta) + \frac{1}{r} \frac{\partial}{\partial \theta} E_r \qquad (1)$$

$$\frac{\partial E_\theta}{\partial t} = - \frac{c^2}{r} \frac{\partial}{\partial r} (rB_\phi) - \frac{J_\theta}{\varepsilon_o} - \frac{\sigma}{\varepsilon_o} E_\theta \qquad (2)$$

$$\frac{\partial E_r}{\partial t} = \frac{c^2}{r \sin\theta} \frac{\partial}{\partial \theta} (\sin\theta B_\phi) - \frac{J_r}{\varepsilon_o} - \frac{\sigma}{\varepsilon_o} E_r \qquad (3)$$

The initial source of EMP from a surface burst is the gradient in the radial Compton current, J_r, at the ground-air interface. In the air away from the ground

$$E_r \sim - \int_o^t \frac{J_r}{\varepsilon_o} dt \qquad (4)$$

---

* At the ground, $- E_\theta$ is equivalent to E_z in the previous graphs.

at early times. In the ground J_r is zero so E_r is small. For simplicity we can consider the ground to be a perfect conductor and set E_r to zero. This θ-gradient in E_r generates a magnetic field through the last term in Equation 1. The B_ϕ generated by E_r varies with height so it couples back into the E_r equation through the $\partial B_\phi/\partial\theta$ term causing the disturbance to propagate upwards at the speed of light.

The initial Compton current pulse is generally only a few tens of nanoseconds wide. Thus at a fixed instant in time there is a large radial variation in J_r over a length of 10 meters or less. The spacial gradient due to the time rate of change of the Compton current is much larger than the spacial gradient associated with the gradual fall off of intensity with range which has a gradient length of about 250 meters. The radial variation in B_ϕ drives E_θ according to Equation 2. E_θ varies with the height and radius since B_ϕ does. The radial variation in E_θ couples back into the B_ϕ equation and causes a wave to propagate in the r-direction at the speed of light. The outgoing waves travel in phase with the γ-pulse and so the signal at a given radius has contributions from all the inner radii at very early times.

Since the Compton current is largest at the inner radii, the fields at a given radius are most strongly driven by waves launched close to the burst point. This situation holds until the air conductivity builds up to the point where it attenuates the waves generated at the smaller radii enough to make up for their larger initial amplitude. To be effective the conductivity only needs to attenuate the wave somewhat faster than the γ-pulse is being attenuated. Conductivity damps an electric field with an e-folding time of ε_0/σ or a distance of $2/\sigma Z_0$ where $Z_0 = 377\Omega$ is the impedance of free space. Assuming an attenuation length of 250 meters for the γ-pulse we find

$$\sigma_\lambda = 2/(250\times377) \tag{5}$$

$$\sigma_\lambda = 2\times10^{-5}\ \text{mho/m} \tag{6}$$

This relatively low level of ionization is reached very early in the pulse at the inner radii. It only requires a dose of about 1 rad in less than 10 nanoseconds or a dose rate of about 10^8 rads/sec. Referring to Figure 6 we see that the 2×10^{-5} mho/m level is reached at 1.2 km at about 60 ns (retarded time). Figure 3 shows that peak conductivities in excess of 2×10^{-5} mho/m extend out to about 1.8 km. When the conductivity at a point reaches a few times 2×10^{-5} the point is electromagnetically isolated from other distant points.

So at very early times the EMP at a fixed radius is generated primarily from regions closer to the burst. This is what Longmire[6] refers to as the wave phase. As the conductivity begins to exceed 2×10^{-5} mho/m at the inner radii, their contribution to the EMP at the larger radii decreases. The EMP keeps increasing but not as fast as before. This is what Longmire refers to as the attenuated wave phase. When the conductivity reaches 2×10^{-5} mho/m at the actual radius where the EMP is being computed the contribution from all inner radii are being damped, and the EMP is being generated locally. Longmire calls this the λ-saturation phase.

During these phases the conductivity is high enough that the attenuation length is smaller than 250 meters but not high enough that the displacement current is small compared to the conduction current. Consequently the radiated fields, E_θ and B_ϕ, have nearly their free field ratio of c. The conduction current and displacement current become comparable when the relaxation time, ε_o/σ, is comparable to the rise rate of the electric field. If we take as a rise time 5×10^{-9} seconds the value of sigma is

$$\sigma_d = 2\times10^{-3} \text{ mho/m}$$

This is the onset of what Longmire refers to as the diffusion phase. In the diffusion phase the electric field saturates and begins to fall while the

magnetic field keeps increasing. Eventually the ratio of E_θ to B_ϕ becomes much smaller than the free field value of c. Referring to Figures 1 and 2 we see that the ratio of peak E_θ to peak B_ϕ is smaller than c out to about 1300 to 1400 meters. At 500 meters the ratio is only about 0.1 c. The peak value of sigma exceeds 2×10^{-3} out to a range of about 900 meters for the 50 kT case we are considering.

The inner edge of the source region, as we have defined it here, is well into λ-saturation at the peak in the γ-pulse but not quite into the diffusion phase. Thus during the rise of the pulse we would expect E_θ to be about equal to cB_ϕ. At the peak in the γ-pulse B_ϕ stops increasing as fast as it was during the rising portion of the γ-pulse. To see the behavior of B_ϕ we examine Equation 3. Near the ground-air interface both σE_r and the radial displacement current are small because of the shorting effect of the ground. Then

$$B_\phi \approx -\mu_o \int_{\theta'}^{\pi/2} J_r \, r d\theta \tag{7}$$

where we have set $\sin\theta = 1$ near the ground. Thus

$$B_\phi \approx \mu_o J_r \delta \tag{8}$$

where $\delta = r(\pi/2-\theta')$ is the effective distance above the ground over which E_r is reduced due to the presence of the ground-air interface. This is approximately a skin depth

$$\delta = \sqrt{\frac{\tau}{\mu_o \sigma}} \tag{9}$$

Above a skin depth the charge carried outwards by the Compton current returns to the burst area as a conduction current through the air. Within a skin depth of the ground the current flows to the ground and returns as a surface current. δ is about 3 meters at the peak of the γ-pulse for the 1.2 km example we have been considering. The magnitude of B_ϕ depends upon both J_r and the skin depth δ. During the rise in the γ-pulse both J_r and σ are increasing at about the same rate and τ is a constant related to the rise time of the Compton current. Thus B_ϕ increases like the square root of J_r.

After the peak in J_r, both J_r and σ begin to decrease at about the same rate, which would tend to cause B_ϕ to decrease also. But for a decreasing pulse τ is no longer a simple constant assocated with the exponential rise or fall of the pulse. Instead τ varies roughly like the time. Since J_r falls like $1/t$, the skin depth increases about as fast as J_r decreases. The net effect is that B_ϕ remains fairly constant after the peak in J_r and σ as shown in Figures 4, 5, and 6.

E_θ also behaves differently after the peak in J_r. After the peak, the slow rate of change in B_ϕ reduces the displacement current to the point where the conduction current dominates it even for σ as small as 10^{-4} mho/m. Thus Equation 2 becomes approximately

$$\sigma E_\theta \approx -\frac{1}{\mu r} \frac{\partial(rB_\phi)}{\partial r} \tag{10}$$

The spacial variation in B_ϕ is still largely due to its time dependence so we can replace derivatives in r with derivatives in time giving

$$E_\theta \approx \frac{1}{(Z_0\sigma)} \frac{\partial B_\phi}{\partial t} \tag{11}$$

where Z_o is the impedance of free space. Thus E_θ tends to be inductive and follows the time derivative of B_ϕ. The displacement current is not completely negligible however, so E_θ deviates somewhat from Equation 11 especially right after the peak.

At times on the order of several microseconds B_ϕ is changing so slowly in time that the actual spacial variation in B_ϕ due to the attenuations of the drivers is important and E_θ becomes less dominated by the time derivatives of B_ϕ. Also the skin depth increases to the point where almost all of the available radial current flows back along the ground-air interface. Once this occurs B_ϕ must decrease as J_r continues to decrease.

AURORA

The AURORA flash X-ray facility has been used by the Harry Diamond Laboratories (HDL) as a tactical source region simulator. They have been supported in their efforts by Mission Research Corporation (MRC). It was apparent from the beginning of our efforts that some way would be needed to enhance the electric field produced in the AURORA test cell for it to be useful as a tactical source simulator.[7] Several schemes were devised and some were implemented.[7,8,9] Modification to the transmission line design in Reference 8, suggested by HDL, should provide the capability of generating a rapidly rising, threat like, electric field in AURORA.

In our haste to design methods of enhancing the electric field in AURORA, we have neglected to explain fully why the naturally occurring fields in AURORA are inadequate. While some may feel it is obvious, others may not. Also, it is important to understand why they are different from the threat fields. Consideration is being given to designing bigger and faster source region simulation facilities. Understanding AURORA's limitations will help in evaluating the usefulness of these proposed simulators and any modifications that might be made to upgrade AURORA.

Another reason for understanding how the fields are generated in AURORA is that we do a poor job of computing the electric fields using approximations generally used to predict the fields in the nuclear environment. This could cast doubt upon our ability to predict fields in a nuclear environment. It is important to show that we understand why the approximations break down and that the reasons are peculiar to AURORA like simulators. This issue may be important enough to justify a more costly computational technique which can treat the AURORA geometry more accurately.

COMPTON CURRENT IN AURORA

The AURORA fields are generated by four brehmstrahlung sources located about 70" (1.778 m) off of the floor of the AURORA test cell. The test cell is 20 meters long, 4.57 m high, and 13.7 m wide. Figure 7 shows examples of Compton current measurements made in the AURORA test cell using a light weight, directional, Compton current sensor designed by MRC.[10] The design has been modified somewhat from that described in Reference 10. The main difference was that the wiring was arranged into a Moebius loop configuration, like that used by Baum,[11] which gives better noise rejection and doubles the output voltage. Also, the solid outer skin was replaced by a thin screen mesh.

In Figure 8 the AURORA Compton current pulse is compared with the threat Compton current pulse. By choosing the correct location in the AURORA room, one can adjust the amplitudes to agree quite well. The Compton current in AURORA is given approximately by

$$J = 620 \cos\theta/R^2 \quad A/m^2 \tag{12}$$

The constant is adjusted to give good agreement with a 90 kV charging voltage. The range R is measured from the "hot spot" which is located 70" (1.778 m) off the floor on the front wall of the room. The angle θ is measured from the normal to the front wall through the hot spot.

This expression for the Compton current neglects the fact that there are really four separate photon sources located in a square array 2.5 ft (76 cm) on a side. We had felt that the computation of the fields in the AURORA room was not sensitive to the fact that there were four sources as long as one was more than a couple of meters from the hot spot.[12] Chadsey et al[13] and Tumolillo et al[14] showed that results near the hot spot were sensitive to the four sources. Reference 13 implied that it was important to model them throughout the room.

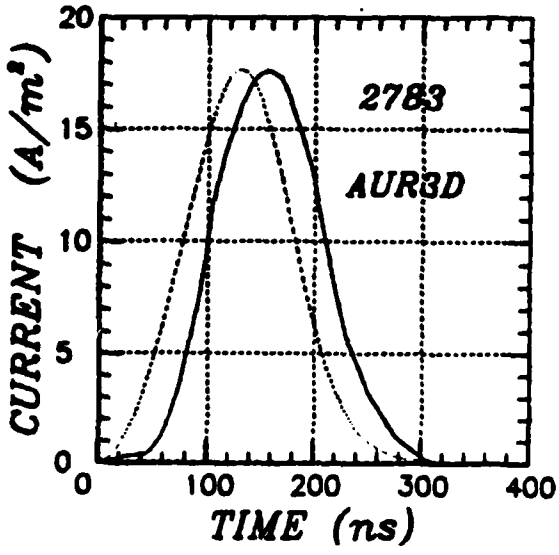

J_z (vertical) on floor
x = -1.5 m, y = 3 m

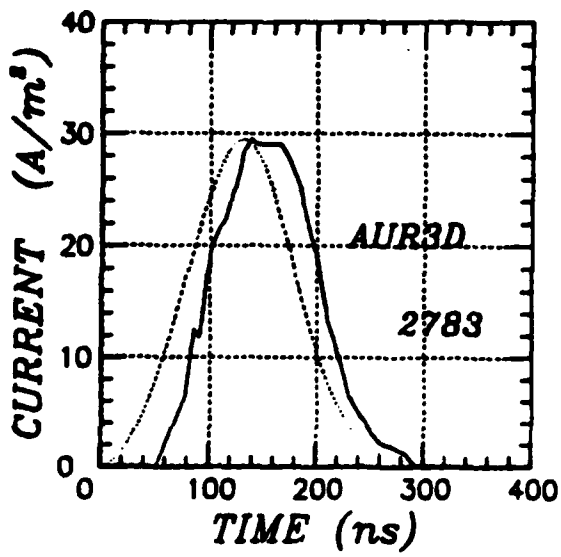

J_x (towards side wall) on floor
x = -1 m, y = 2.5 m

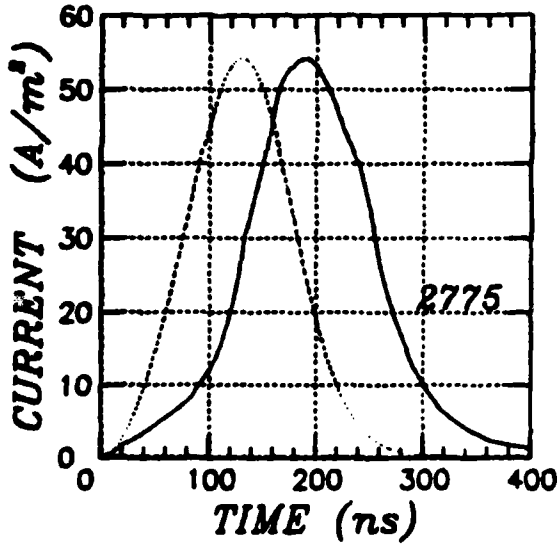

J_y (towards rear of room) on floor
x = -1.5 m, y = 2.5 m

Figure 7. Measured Compton currents in AURORA. Numbers on figures indicate shot number. The Compton current pulse shape used in AUR3D is shown for comparison. It is displaced in time for clarity.

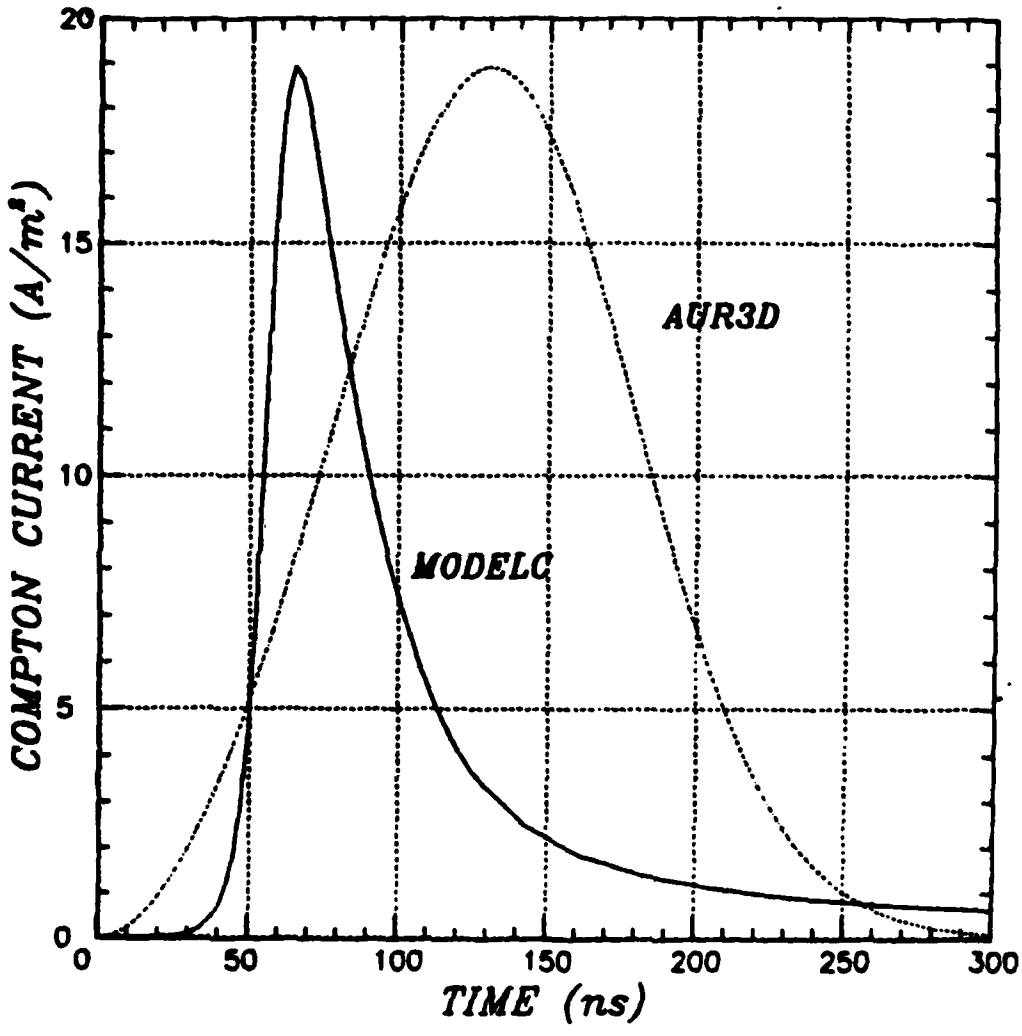

Figure 8. Comparison of typical AURORA Compton current pulse with the threat Compton current pulse computed with MODELC.

Our opinion, that a one source model was adequate, was reinforced by the excellent agreement we obtained between the measured and observed surface magnetic fields as reported in Reference 12. The improvement was obtained by slightly modifying the conductivity gradient near the hot spot - at least we thought it was.

Unfortunately it turned out that the change was the result of a computer error that introduced a small, artificial, divergence of Compton current. As we shall see later, the results are very sensitive to even a small divergence of Compton current. Only the results plotted in Figures 7 and 8 of Reference 12 were affected by the error.

In our effort to improve our computation of the fields and currents in AURORA we developed a four source model for use in the AUR3D computer code. As we shall see later, the four source model gives excellent agreement to the measured surface currents. The equations for the four sources are easily treated with a computer but they make the analysis we need to perform next unduly messy. We will therefore use the one source model (Equation 12) in our analysis.

Using Equation 12 we see that the threat Compton current of 19 A/m^2 would occur about 5.7 m from the hot spot on the centerline through the hot spot. On the floor, to get a horizontal Compton current of 19 A/m^2, one would have to be at a distance of 5.1 meters. At this distance there would also be a vertical Compton current of 6.6 A/m^2. In the sample threat environment developed above, there was no vertical component of Compton current because we were considering a surface burst. We neglected the small amount of Compton current which would be generated by the electric and magnetic fields turning the horizontal Compton current. Thus AURORA more nearly simulates a near surface burst than a surface burst. If this were a major disadvantage one could install a ground plane at the height of the hot spot and conduct experiments on that plane rather than on the floor.

The major shortcoming of AURORA is not the amplitude of the Compton current, indeed it is more than adequate. It is the slow rise of the pulse that is the problem. The differences are apparent in Figure 8. AURORA has Compton current rise time of about 80 ns. Our threat Compton current rises in about 15 ns. The differences are also apparent in Figure 9 where the Fourier transforms of the two pulses are compared.

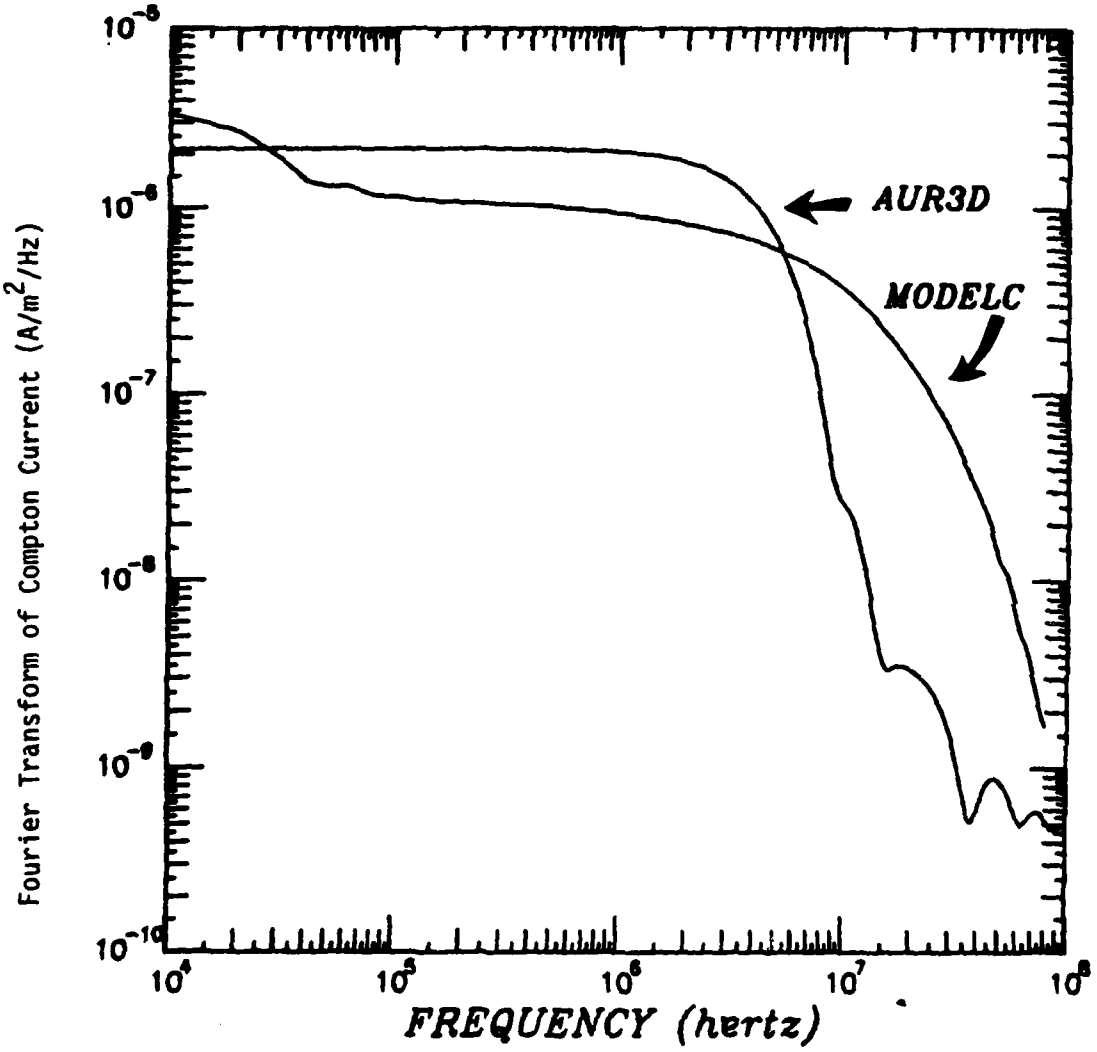

Figure 9. Fourier transform of Compton currents shown in Figure 8. The threat transform from MODELC contains much more high frequency than the AURORA pulse.

MAGNETIC FIELDS IN AURORA

The surface magnetic fields in AURORA were measured at a variety of locations in the AURORA test cell by HDL. The results of these measurements and comparisons with AUR3D computations were made in Reference 12. A model for the currents was developed and presented in Reference 15. Here we will present a simple way to estimate the surface currents to show how they differ from the threat case even though the amplitude of the Compton current is comparable.

Recall that in the threat environment the surface magnetic field is given by

$$H_\phi = J_r \delta \qquad A/m \tag{13}$$

where

$$\delta = \sqrt{\tau/\mu_o \sigma} \tag{14}$$

is a skin depth. In other words the surface current density is just the volume current density times the height over which the surfaces collect the volume current density.

To calculate the skin depth in AURORA we take $\tau \sim 8\times10^{-8}$ seconds. The peak air conductivity varies roughly like

$$\sigma_p = 3\times10^{-2}/R^2 \tag{15}$$

so the skin depth is

$$\delta \sim 1.4\ R \quad m \tag{16}$$

At a distance of 5 or 6 meters, where the Compton current is at about threat magnitude, the skin depth is larger than the height of the AURORA test cell (4.57 m). It is clear that the surface magnetic field in AURORA cannot be defined by Equation 13 since there is not a full skin depth of Compton current to collect. Instead we use

$$H_x = J_r \, \ell \tag{17}$$

where ℓ is an effective collection height. For our simple model we can just assume that the floor collects all the Compton current below the hot spot. So the effective length is 1.778 m. Thus we can approximate the surface magnetic field in AURORA with

$$H_x \approx \frac{620}{R^2} \times 1.778$$

$$H_x \approx 1100/R^2 \quad A/m \tag{18}$$

Figure 10 shows how this simple equation compares with the measured surface currents. A surface magnetic field in the x-direction (across the room) corresponds to a surface current in the y-direction (along the length of the room). The data are indicated with triangles. The dashed straight line is a plot of Equation 18. The agreement is quite good except in very close to the source where the simple model breaks down. The solid curve in Figure 10 is the surface current computed with the four source version of AUR3D. The agreement is excellent at all ranges and is much better than was obtained from the simple one source model used previously Figures 11 through 14 compare measured surface currents in AURORA with those computed with the four source AUR3D model and the single source AUR3D model used previously (Reference 15). In Figure 15 we show some typical surface current measurements made by HDL in the AURORA test cell. Also shown are the AUR3D results at nearby points.

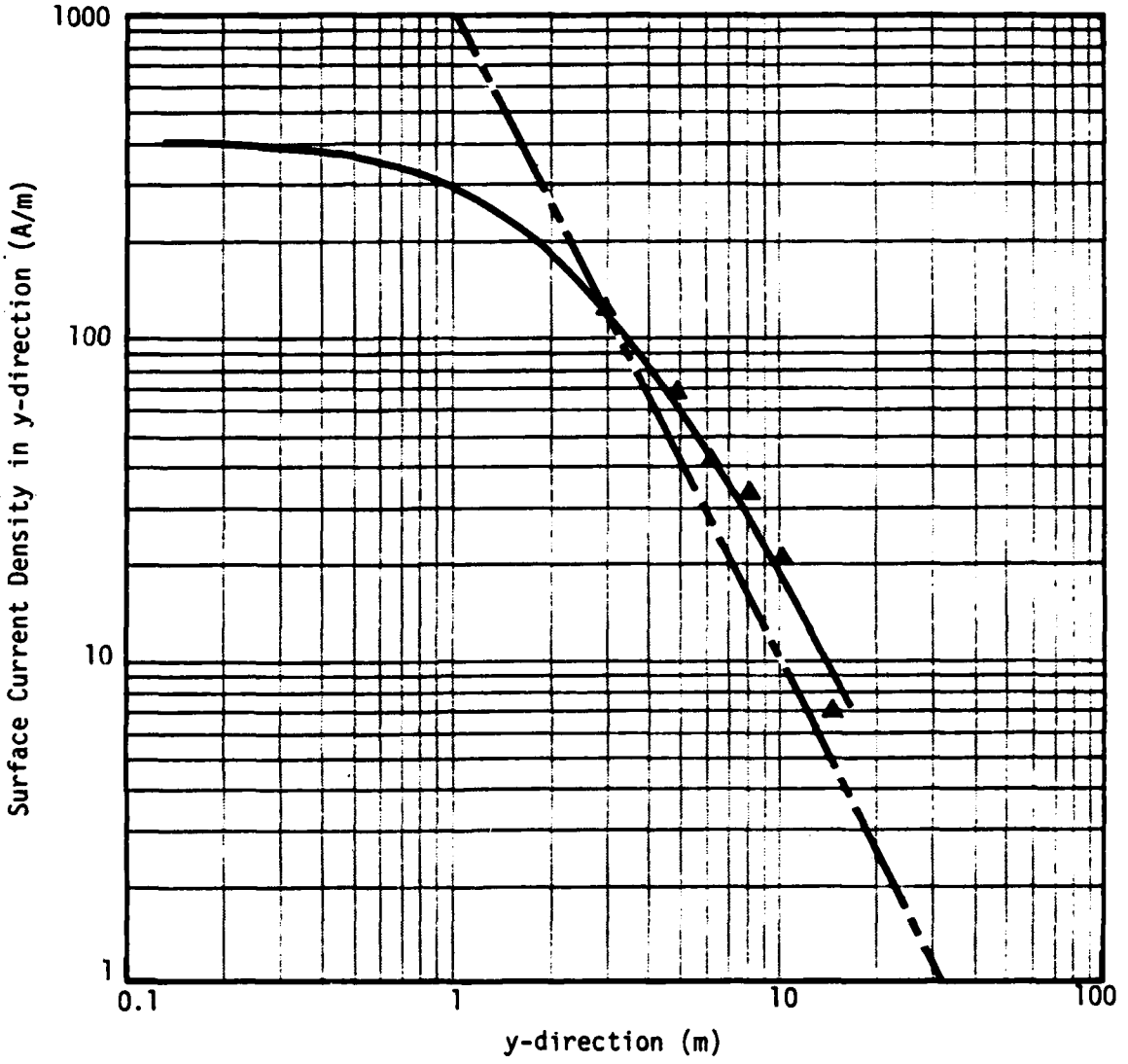

Figure 10. Comparison between data (▲), four source AUR3D model (solid line) and simple model based on Equation 17. Data points are on floor at x = 0. A surface current density in the y-direction (down the length of the room) corresponds to a surface magnetic field in the minus x-direction (across the room or to the left standing at the hot spot facing the rear of the test cell).

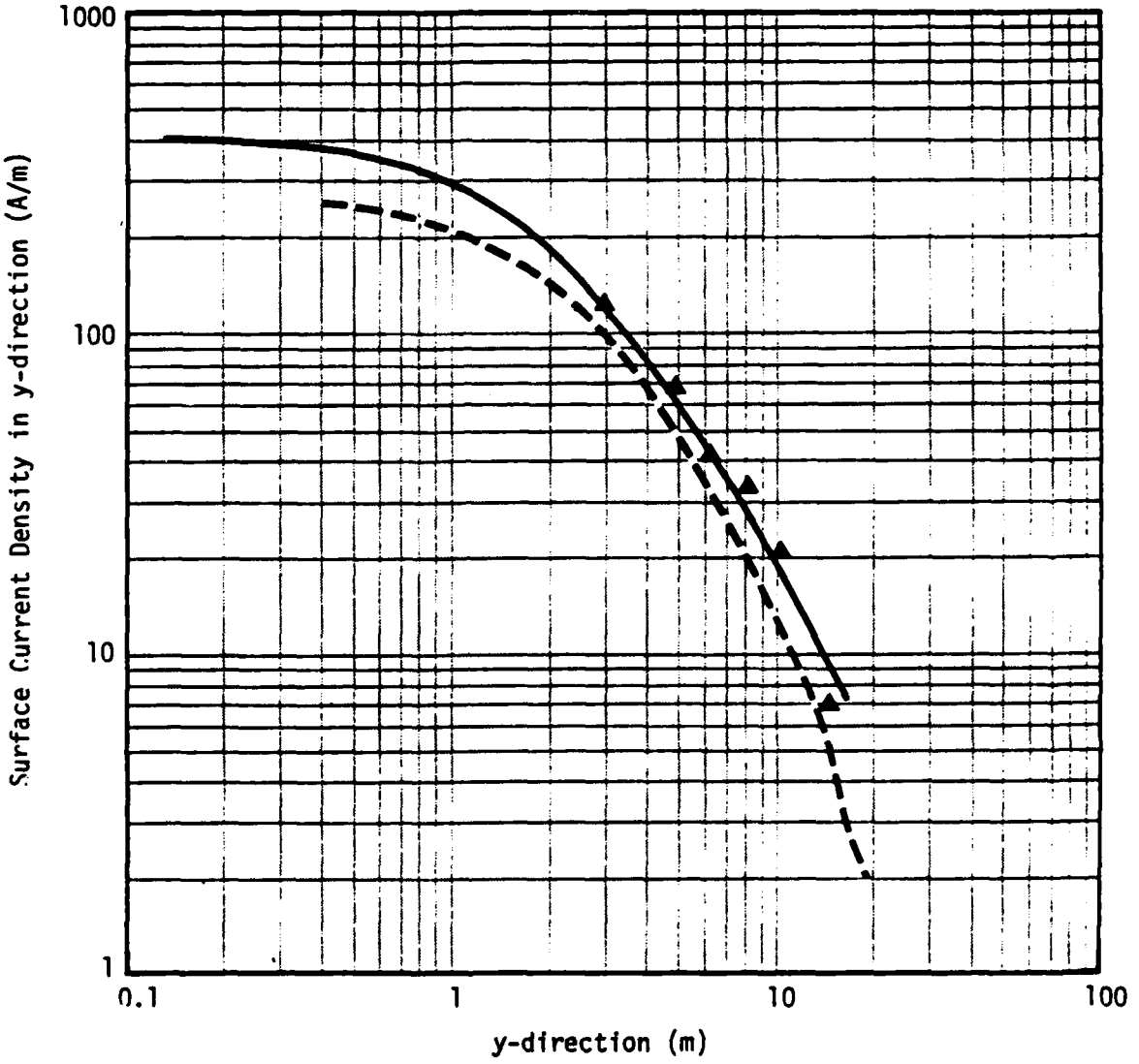

Figure 11. Comparison between data (▲), four source AUR3D model (solid line) and the previous one source AUR3D model (dashed line). Data points are on floor at x = 0. A surface current density in the y-direction (down the length of the room) corresponds to a surface magnetic field in the minus x-direction (across the room or to the left standing at the hot spot facing the rear of the test cell).

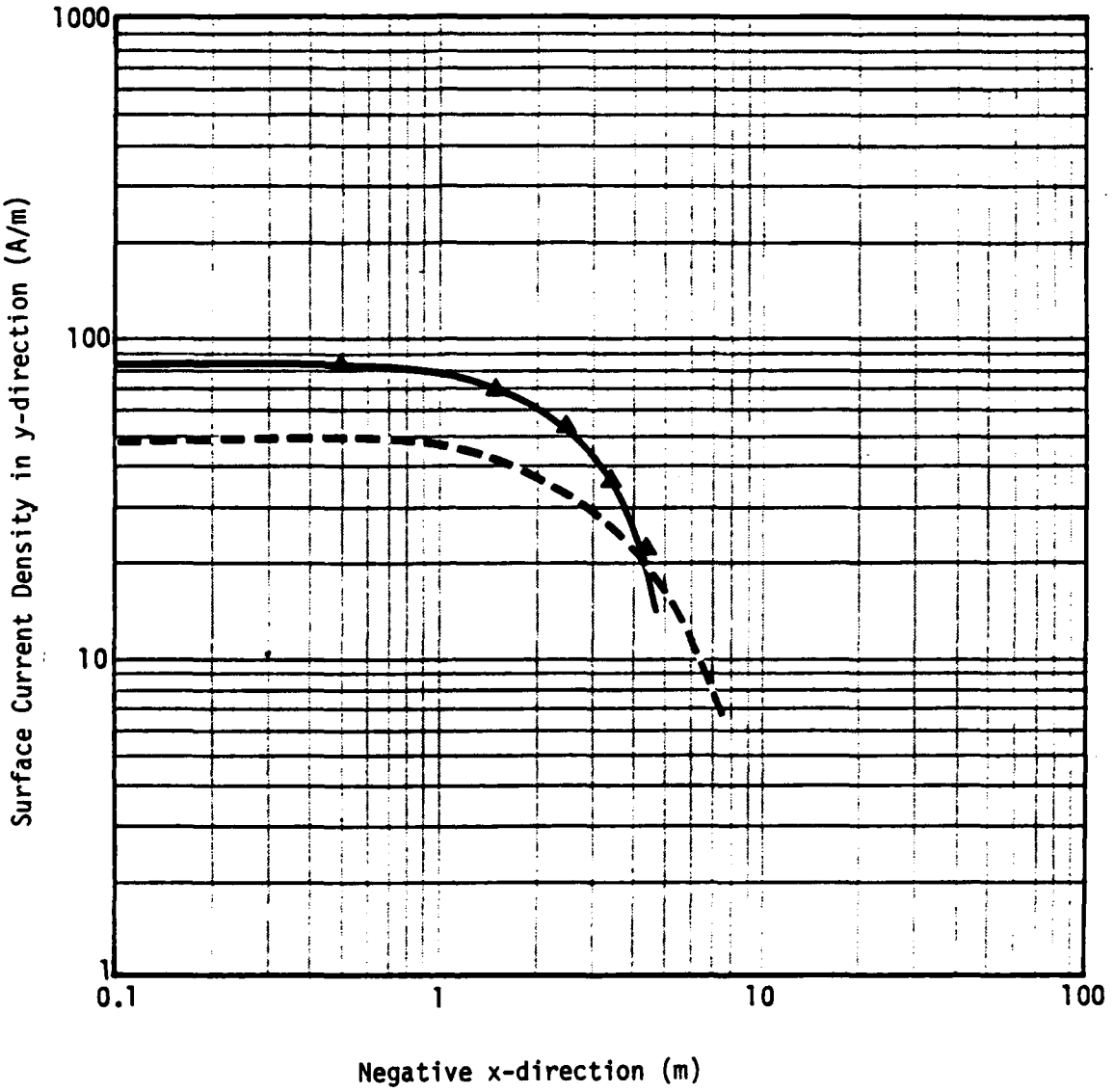

Figure 12. Comparison between data (▲), four source AUR3D model (solid line) and the previous one source AUR3D model (dashed line). Data points are on floor at y = 4 m and at various x-positions across the room.

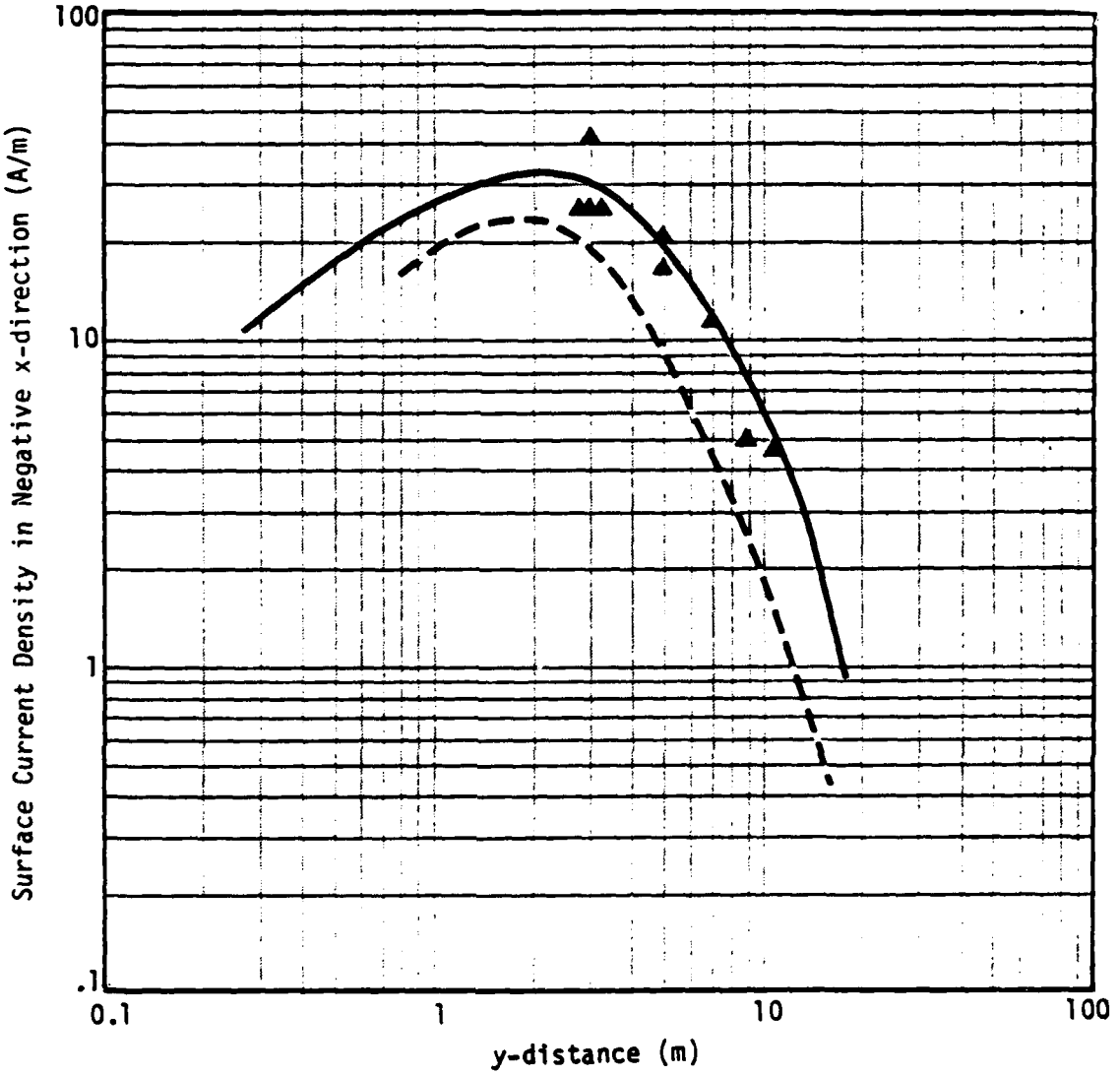

Figure 13. Comparison between data (▲), four source AUR3D model (solid line) and the previous one source AUR3D model (dashed line). Data points are on the floor at x = -2.5 m and at various y-distances down the length of the room. A surface current density in the negative x-direction (across the test cell, to the left facing the rear of the test cell) corresponds to a surface magnetic field in the y-direction (down the length of the AURORA test cell).

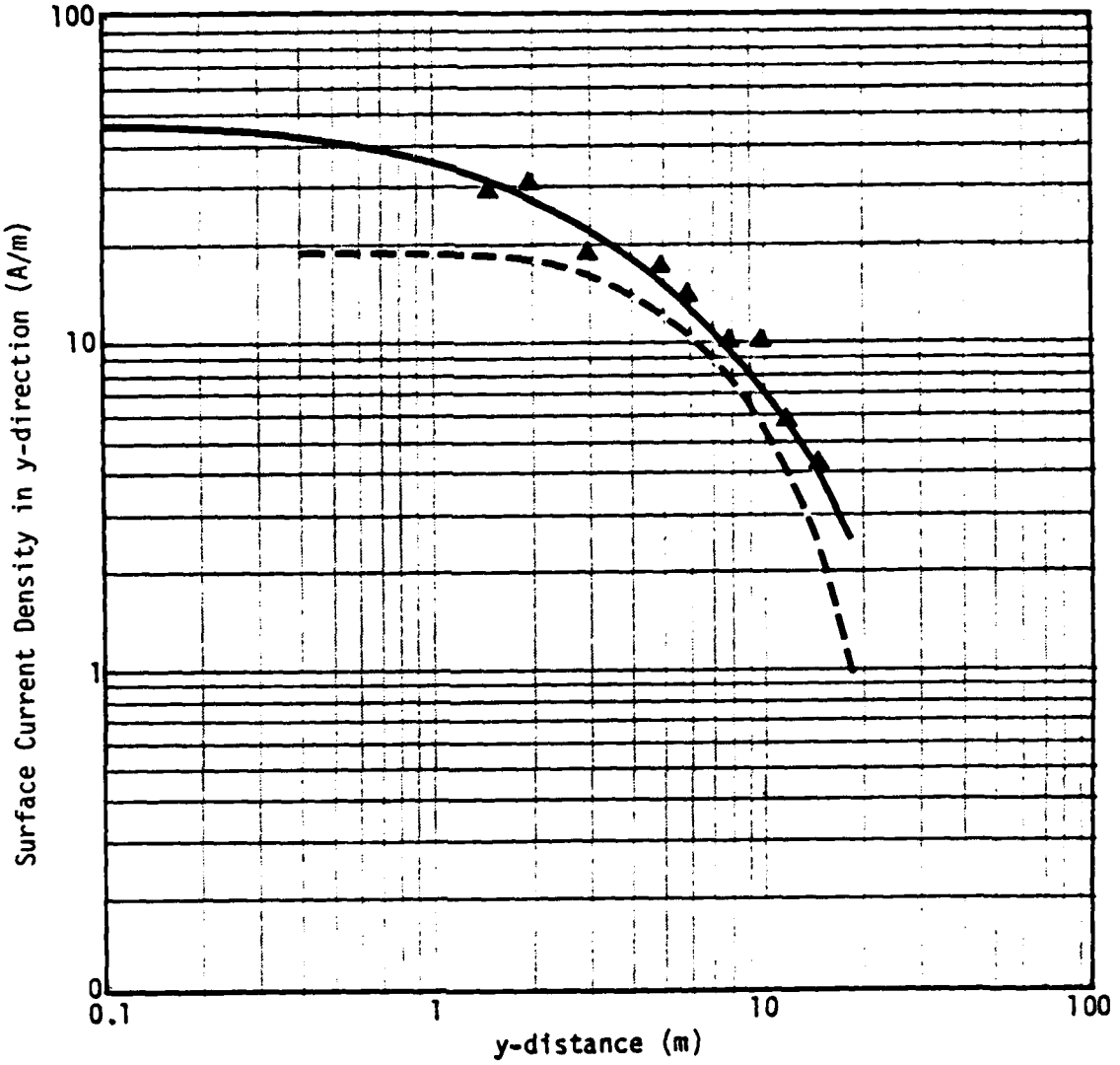

Figure 14. Comparison between data (▲), four source AUR3D model (solid line) and previous one source AUR3D model (dashed line). Data points are on the side wall (x = 5.5 m) at the height of the hot spot and at various positions down the length of the room. On the wall, a surface current density in the y-direction corresponds to a surface magnetic field in the negative z-direction (down towards the floor).

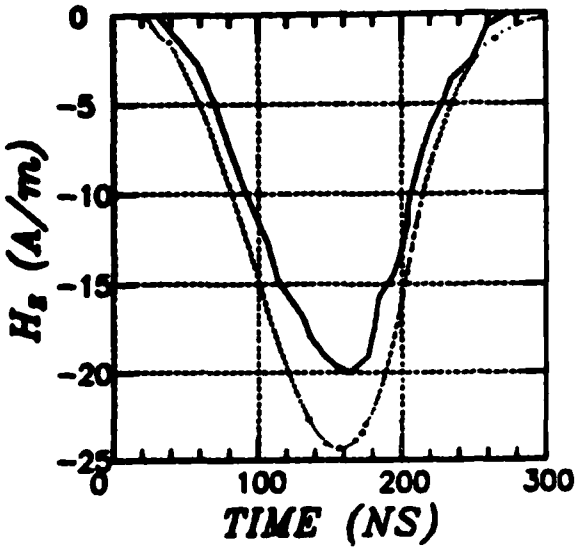

y = 3 m, Shot 2423

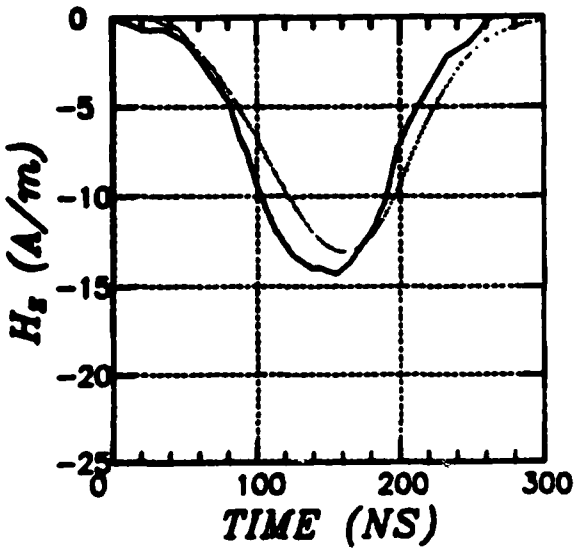

y = 6 m, Shot 2426

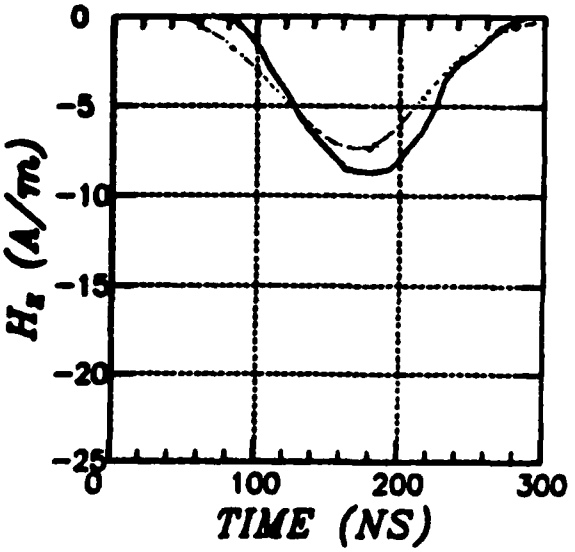

y = 10 m, Shot 2428

Figure 15. Typical surface current density wave forms (solid line) compared with AUR3D results (dotted line). All data points are on side wall (x = -5.8 m) at height of hot spot. They measure the flow of surface current down the length of the wall (y-direction). A negative H_z corresponds to a positive surface current.

Again the agreement is quite good. The excellent agreement with the four source model at such a wide range of location suggests that we have reasonable good model for the Compton current sources in AURORA. The agreement with simple theories shows that we understand the mechanisms which determine the surface currents.

In Figure 16 we compare a computed AURORA pulse with that computed for the threat environment. As expected, the threat pulse rises faster and remains higher at late times. Also, the threat pulse is higher for the same peak Compton current. To get about the same peak surface current in AURORA, we had to move in to a distance of about 3 meters instead of 5 meters where the Compton currents are comparable. In Figure 17 the Fourier transforms of the two pulses are shown. As one would expect, the threat pulse has a larger amplitude at both low and high frequencies.

The differences between the currents in AURORA and in a threat environment are in part due to the slow rise of the AURORA pulse and in part due to the limited size of the AURORA test cell. If the AURORA pulse rose faster, the skin depth could be smaller than the room dimensions and the magnetic field would be correct at early times. However, even if the rise time were perfectly realistic, the finite extent of the source would eventually limit the surface magnetic field. If there were no top on the AURORA test cell, the surface current on the floor could be increased, but the collection height would still be limited to something like the distance from the source or about 5 meters in the case of AURORA. In our threat environment the collection height extends up to 1200 m at late times.

Since the collection height in AURORA is essentially constant, the surface magnetic field follows the Compton current during both its rise and fall. In the threat environment the magnetic field rises slightly slower than the Compton current on the rise since the skin depth is gradually decreasing. But after the peak in the air conductivity the skin depth increases and the

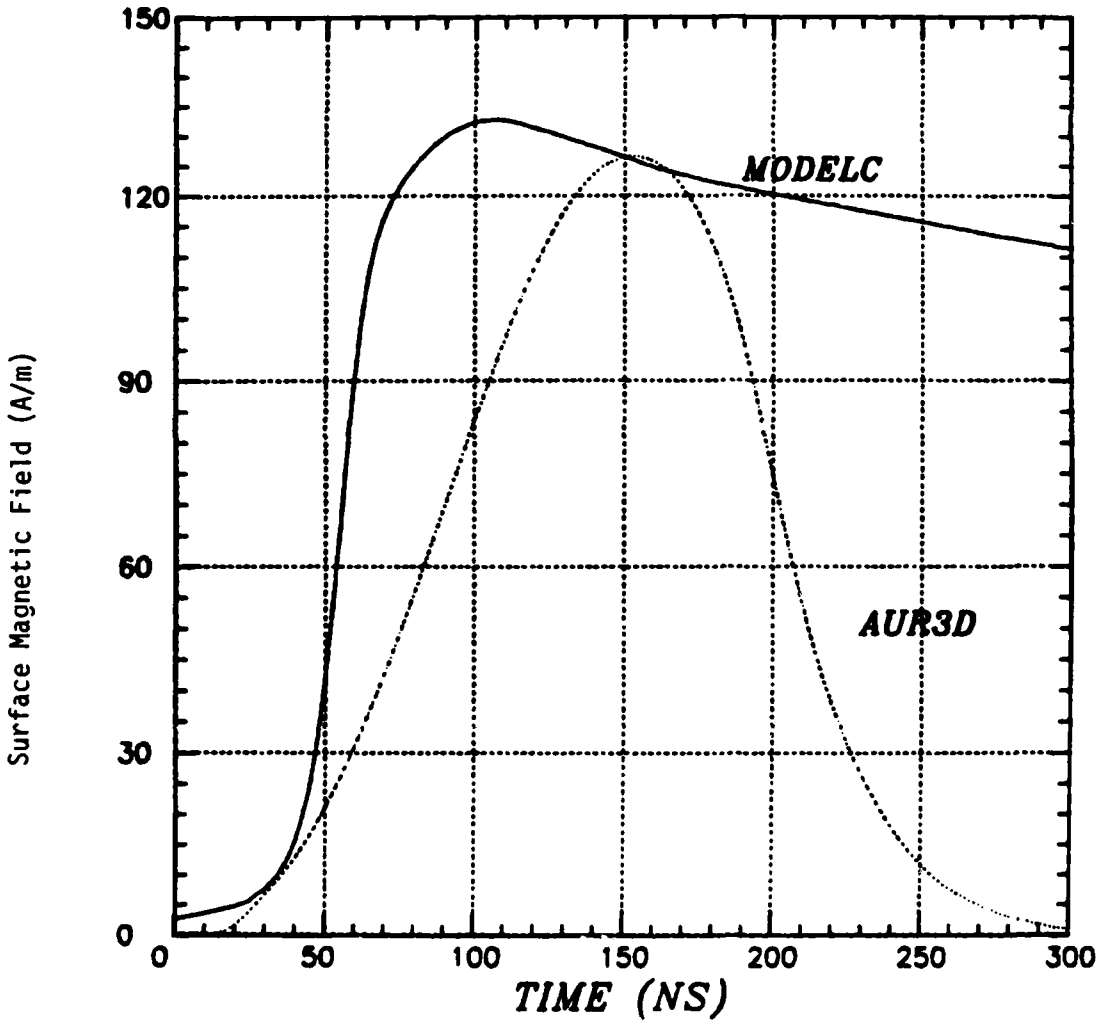

Figure 16. Comparison between the surface magnetic field in AURORA (as computed with AUR3D) and the threat magnetic field computed with MODELC. The AUR3D result is on the floor at x = 0 and y = 2.9.

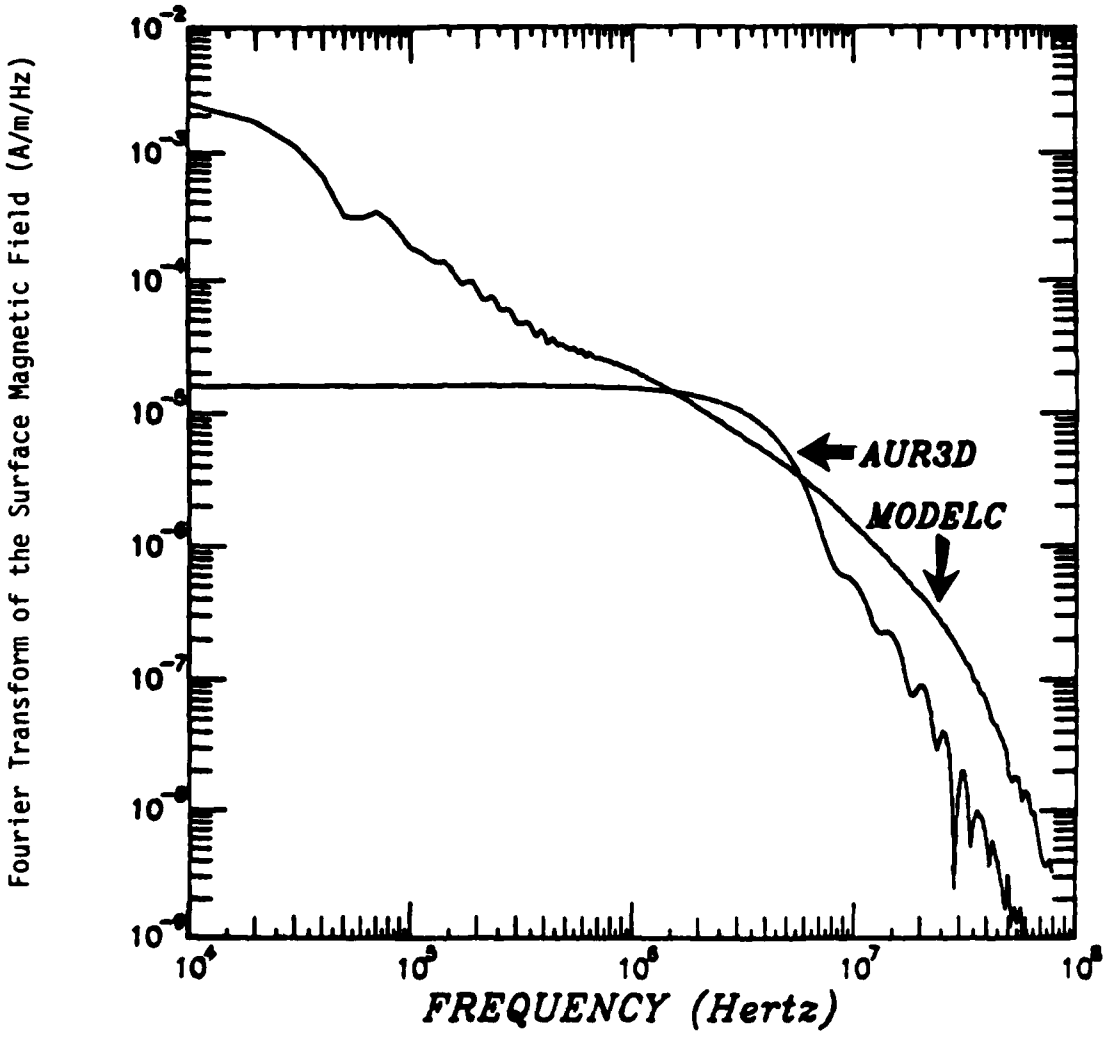

Figure 17. Comparison between the Fourier transforms of the surface magnetic field shown in Figure 16. Note the lack of high frequency content in the AUR3D results.

surface magnetic field continues to increase and maintain a large value even though the Compton current decreases significantly. Only after times on the order of about 20 μ-seconds does the surface magnetic field fall. This occurs when the skin depth is comparable to the radius of the observer. A further increase in the skin depth does not increase the surface current because all of the Compton current is already being collected. Any source region simulator will face this problem, it is not peculiar to AURORA.

ELECTRIC FIELDS IN AURORA

For most of the system applications that HDL is considering using AURORA for, the electric field is the dominant driver of the system. It was shown above that the surface magnetic fields in AURORA had threat level amplitudes although the pulse shape was not very realistic. One might expect that the electric fields in AURORA would also have threat level amplitudes. Unfortunately they are about an order of magnitude too small. Also, one might expect that since our calculations of the surface magnetic fields are so accurate, we should be able to accurately compute the electric fields in AURORA. Unfortunately that is not the case as we shall see below.

In order to understand why the electric fields in AURORA, both measured and computed, are much smaller than the threat fields we will develop a simple model for estimating the electric fields in all three cases. The starting point for the model is Poisson's equation:

$$\varepsilon_o \vec{\nabla} \cdot \vec{E} = \rho. \tag{19}$$

Using Gauss's law we can relate the surface normal electric field, E_z, to the charge in the air above the surface:

$$E_z = \frac{\rho}{\varepsilon_o} \ell, \tag{20}$$

where ℓ is a length to be determined. This simple model assumes that near the surface the fields are nearly vertical.

Taking the divergence of Equation 2 and using Equation 19 we obtain an expression for ρ:

$$\frac{\partial \rho}{\partial t} + \frac{\sigma \rho}{\varepsilon_o} = - \vec{\nabla} \cdot \vec{J} - \vec{E} \cdot \vec{\nabla} \sigma \ . \tag{21}$$

The $\sigma\rho/\varepsilon_0$ term is not a source term for creating charge. It acts to relax any charge built up in a time of ε_0/σ. Taking 8×10^{-8} seconds as a characteristic time in AURORA, we see that the relaxatior term will be important in AURORA when σ exceeds about 10^{-4} mho/m. In the threat environment the characteristic time during the rise of the pulse is more like 10^{-8} seconds so σ must get up to about 8×10^{-4} mho/m for the relaxation term to dominate. After the peak in the Compton current the relaxation term can be important at lower conductivities.

The $\vec{E}\cdot\vec{\nabla}\sigma$ term actually generates a space charge. To see this imagine a volume in space with a uniform electric field. Assume that the conductivity is higher on one side of the volume than on the other. Then more conduction current will flow into the volume on the side where σ is high than flows out on the side where it is small. This leads to an accumulation of charge in the volume. In AURORA the initial radial electric field is positive. The conductivity decreases with distance from the sources so $\vec{\nabla}\sigma$ is negative. Thus $\vec{E}\cdot\vec{\nabla}\sigma$ term tends to generate a positive space charge for as long as E-radial stays positive. In AURORA σE is somewhat smaller than J. As we shall see below the length scale for the divergence of J is about 25 meters. So for the $\vec{E}\cdot\vec{\nabla}\sigma$ term to be important the gradient length for $\vec{\nabla}\sigma$ would have to be somewhat smaller than that or say about 5 meters. Actually the importance of the term is reduced even further because $\vec{E}$ and $\vec{\nabla}\sigma$ are not parallel. It is important in the first 3 m or so of the AURORA room.

In the threat environment the gradient length for σ is related to the attenuation length of the Compton current which is about 250 meters. Thus the $\vec{E}\cdot\vec{\nabla}\sigma$ term is negligible for the threat environment.

The $\vec{\nabla}\cdot\vec{J}$ term can be divided into two parts. Even if the spacial variation of the Compton current is divergence free, there is still a divergence of J from the time variation of J. To see this picture a volume in

space in which a spacially uniform Compton current flows. If J is increasing in time more current will have entered the front of the volume than has left the rear of the volume leading to an accumulation of charge. For this retarded time effect we can write

$$\vec{\nabla}\cdot\vec{J} = -\frac{1}{c}\frac{\partial \vec{J}}{\partial t} \tag{22}$$

In AURORA the time derivative of the Compton current is about an order of magnitude smaller than for the threat at the same peak amplitude.

A second source of a divergence of J occurs if the spacial variation of J is divergent even at a fixed retarded time. For our AUR3D code calculations we assume that the Compton current at a point is proportional to the photon flux at that point. The only spacial divergence is due to the attenuation of the photon flux as it is absorbed by the air. The attenuation length for this is about 250 meters as in the threat case. It is much longer than the room dimension of 20 meters. It is also much larger than the $c\tau$ length of 25 meters associated with the time variation of the Compton current discussed above.

Unless one takes special precautions an artificial divergence of J will be generated in computer codes used to solve for the fields in the AURORA test cell. (In fact, it can happen even if you think you are being careful -as it did to us in Reference 12.) We average J over the whole face of each finite difference cell to keep the spatial divergences small in the AUR3D code.

Over the bulk of the AURORA room we assume that

$$\frac{\partial \rho}{\partial t} + \frac{\sigma\rho}{\varepsilon} \approx \frac{1}{c}\frac{\partial J}{\partial t} \tag{23}$$

This is a good approximation in the threat environment and we assume it is in the AURORA test cell.

At early times the air conductivity is negligible giving

$$\rho \sim \frac{J}{c} , \tag{20}$$

so we have

$$E_z = Z_o J \ell , \tag{21}$$

where we have used

$$Z_o = 120\pi = 1/\varepsilon_o c \tag{22}$$

In the threat environment ℓ is just a skin depth. Thus E_z, like B_ϕ, is proportional to the radial Compton current times the skin depth. In fact the ratio between the two is the speed of light as one would expect at low levels of air conductivity. In AURORA the appropriate length is the distance to the center of the space charge which is only 1.778 m, much less than a skin depth. In AURORA we would expect the early time surface normal electric fields to be pointing in, towards the negative charge in the room, on all surfaces including the floor and ceiling.

We can estimate a maximum value for the vertical electric field in the absence of air conductivity using Equations 12 and 21 and ℓ = 1.778 m:

$$E_z = \frac{4.2\times10^5}{R^2} \text{ V/m} . \tag{23}$$

Thus, even in the absence of air conductivity, we would not expect threat level fields (> 30kV/m) in AURORA beyond 4 meters from the hot spot. At a distance of 10 meters the E-field would be down to 4.2 kV/meter.

If the air conductivity increases beyond 10^{-4} mho/m or so, the conduction current will significantly reduce the charge in the air. If the conductivity term dominates then

$$\rho = \frac{\varepsilon_0}{\sigma c} \frac{\partial J}{\partial t} \quad , \tag{24}$$

and

$$E_z = \frac{\ell}{\sigma c} \frac{\partial J}{\partial t} \tag{25}$$

Taking $\ell = 1.778$ m, $c\Delta t \sim 24$ m, and $\sigma = \frac{1}{2} \sigma_{peak}$ gives

$$E_z \sim .14 \ (J/\sigma)_{peak} \tag{26}$$

The exact value of J/σ varies depending upon field strengths and the water vapor content of the air. A typical value is 30 kV/m. Thus we could expect

$$E_z = 4.3 \text{ kV/m} \tag{27}$$

in AURORA. Note that Equation 27 predicts that the peak value of E does not depend upon the location in the AURORA test cell as long as the conductivity is high enough that Equation 24 is satisfied.

In the threat environment the air conductivity term is not as important as it is in AURORA because the pulse rises so much faster. At the peak air conductivity, 3.5×10^{-4} mho/m, the relaxation time is still 25 ns. This is short enough to cause a rapid drop in E but not enough to cause a sign reversal.

This model suggests that the electric fields generated by AURORA could be made larger by increasing the rise rate of the pulse. Also E could conceiveably be increased by removing the ceiling so that the floor would collect a greater height of charge. This would probably not be feasible at AURORA but should be considered in any new facility.

Figure 18 shows the electric field computed at several locations in the AURORA test cell. It is seen that the peak amplitude is fairly constant. The peak magnitudes are in good agreement with our simple model. As predicted by Equation 25, the electric field peaks on the rising part of the Compton current pulse where $\partial J/\partial t$ is large. The electric field is small near the peak in the Compton current because $\partial J/\partial t$ is small and the air conductivity is large. After the peak in the Compton current the electric field goes slightly negative because $\partial J/\partial t$ is negative. The negative excursion is smaller than the initial positive peak because the AURORA pulse falls more slowly than it rises. Also, the positive peak is enhanced somewhat by the charge that accumulates before σ builds up. The field stays negative at late times because the falling air conductivity traps charge in the room.

Figure 19 shows examples of electric fields actually measured in the AURORA test cell. They bear almost no resemblance to the fields computed using AUR3D. The peak magnitudes are not far off but the measured E-fields follow the Compton current. They peak when the AUR3D fields are near zero. The discrepancy is not due to a coding error. The above analysis shows that the computed fields are quite reasonable given the sources used by AUR3D.

The most likely explanation for the discrepancy is that there is a significant spacial divergence in the Compton current. The Compton electrons generated by the MeV range photons in the AURORA test cell have a range of about 1 meter. The Compton current at a point in the test cell is the vector sum of the current from individual Compton electrons born within an electron range of that point. If the photon flux varies significantly over the range of a Compton electron, errors can be generated if one assumes that the Compton current is proportional to the photon flux at that point.

In the threat environment the part of divergence of J related to the retarded time effects has a length scale $c\tau \sim 3$ m. The photon flux varies over a length of 250 m so one is safe in assuming that the Compton current is proportional to the photon flux.

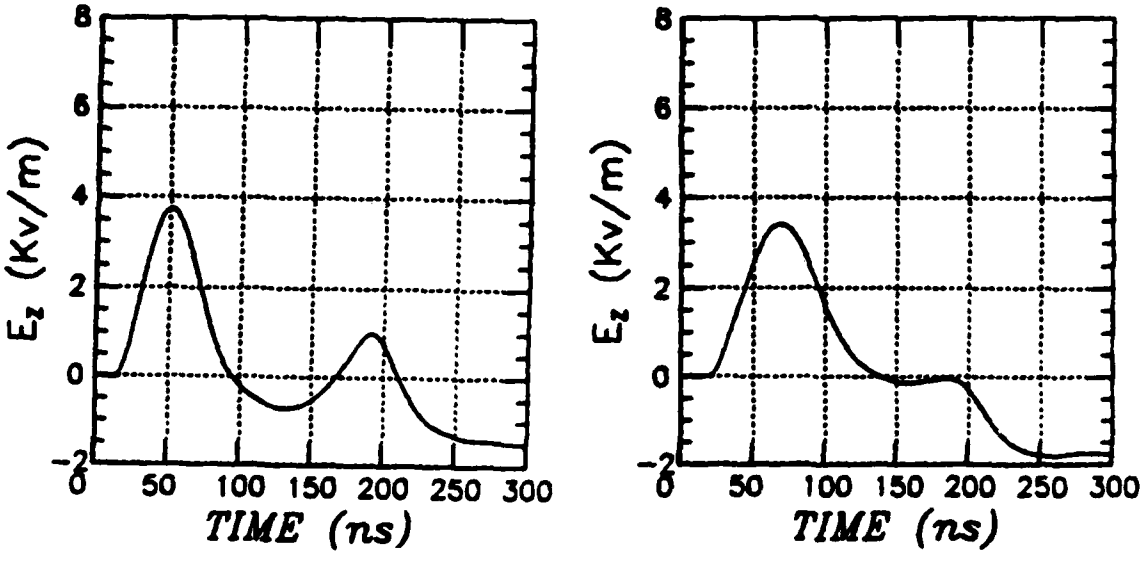

y = 3.15 m

y = 5.00 m

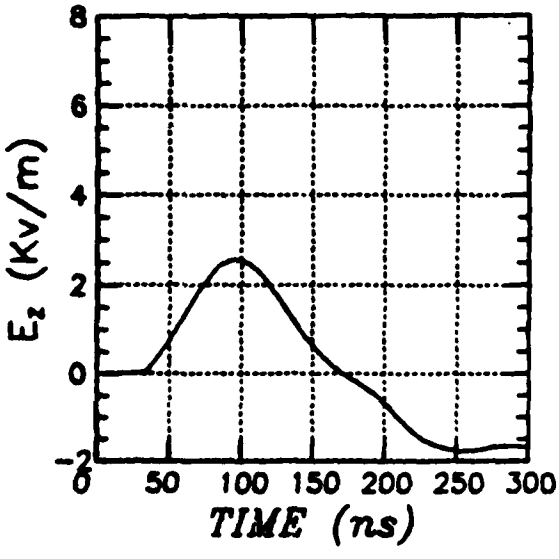

y = 8.37 m

Figure 18. Examples of surface normal electric fields on the floor of the AURORA test cell computed with AUR3D.

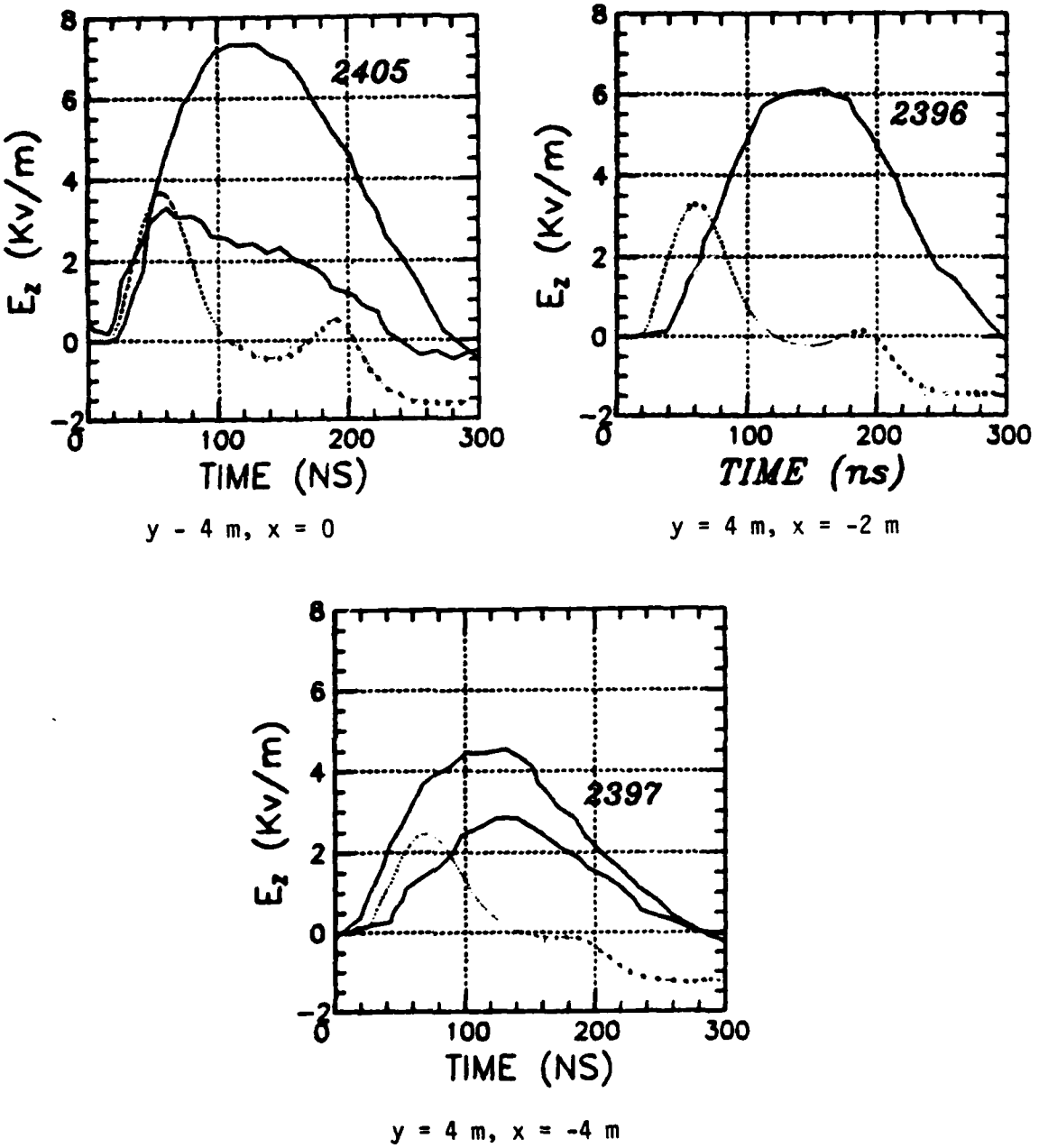

Figure 19. Examples of measured surface normal electric fields in AURORA. Corresponding AUR3D results are shown in dots for comparison. In two of the cases shown, two different electric field sensors were used. See Reference 17 for details of the sensors. The AURORA shot numbers are indicated on each graph.

In AURORA the length scale $c\tau$ is more like 24 m. The source intensity varies roughly like the distance from the source. A deviation from a divergence free Compton current with a length scale of only 10 m or so would be sufficient to explain the observed E-field behavior. If the gradient length is L then

$$\nabla \cdot J \sim J/L \tag{28}$$

and

$$E_z \sim \frac{J}{\sigma} \frac{\ell}{L} \tag{29}$$

Taking $J/\sigma \sim 30$ kV/m and $\ell \sim 1.778$ m we see that if $L = 10$ m, E_z would be large enough to explain the observed fields. Note that a spacial divergence of J leads to an electric field for which $\sigma E \propto J$ and not $\partial J/\partial t$ as was computed with AUR3D.

One can in principle compute the Compton current at a point from a given photon flux without assuming that the two are proportional. The usual techniques involve injecting large numbers of Compton electrons and following their trajectories as they scatter and slow down. The cost of doing this in 3-D can be quite expensive. A recently developed fluid like treatment of SGEMP electrons may provide a less expensive method for computing accurate Compton currents.[16]

The costs of doing this needs to be traded off against the fact that the AURORA fields will most likely <u>not</u> be used to drive various systems. Field enhancement techniques such as low impedance transmission lines are more likely to be used. The benefits of performing the calculation would be to verify that one can indeed compute the AURORA fields and that there are no fundamental physical processes involved that would impact our ability to

accurately predict fields in a nuclear environment. The computations would also be useful if one were considering modifying AURORA to enhance its performance. This $\vec{\nabla}\cdot\vec{J}$ effect is a fundamental limitation of any simulator although it would be reduced in significance if the pulse rose faster.

It is interesting to note that close to the AURORA source, where $\vec{E}\cdot\vec{\nabla}\sigma$ dominates the $\vec{\nabla}\cdot\vec{J}$ term, AUR3D does a much better job of fitting the data as shown on Figure 20. Note the double peaks observed in both the data and code results. The addition of a source following the shape of the Compton current pulse is still needed to get the agreement to be satisfactory.

The measured surface normal electric field in AURORA is compared with the threat field in Figure 21. The measured field is about a factor of five smaller in peak amplitude and has a much slower rise. This is shown clearly in Figure 22 where the Fourier transforms of the two wave forms are compared. The lack of high frequency content in the AURORA pulse is evident. The rapid variation in the high frequency part of the transform of the data is an artifact of the digitizing process.

Many objects of interest respond to the sum of the displacement current, $\varepsilon_0\dot{E}$, and the conduction current σE. For example, this is the dominant drive of the whip antennas HDL has been testing in AURORA. In Figure 23 the two currents and their sum are shown for the threat environment. The displacement current is bipolar and dominates at early times. It has a peak value of 14 A/m^2. The conduction current dominates immediately after the peak in the electric field and has a peak value of 10 A/m^2. At later times the two currents oppose each other and are nearly equal. The displacement current is slightly larger in magnitude.

Figure 24 shows a similar result for AURORA, on the floor 4 meters out from the front wall. The displacement current, shown as a dashed line, peaks at about 1.5 A/m^2 or about an order of magnitude smaller than that for the threat case. The conduction current peaks at 34 A/m^2 which is more than

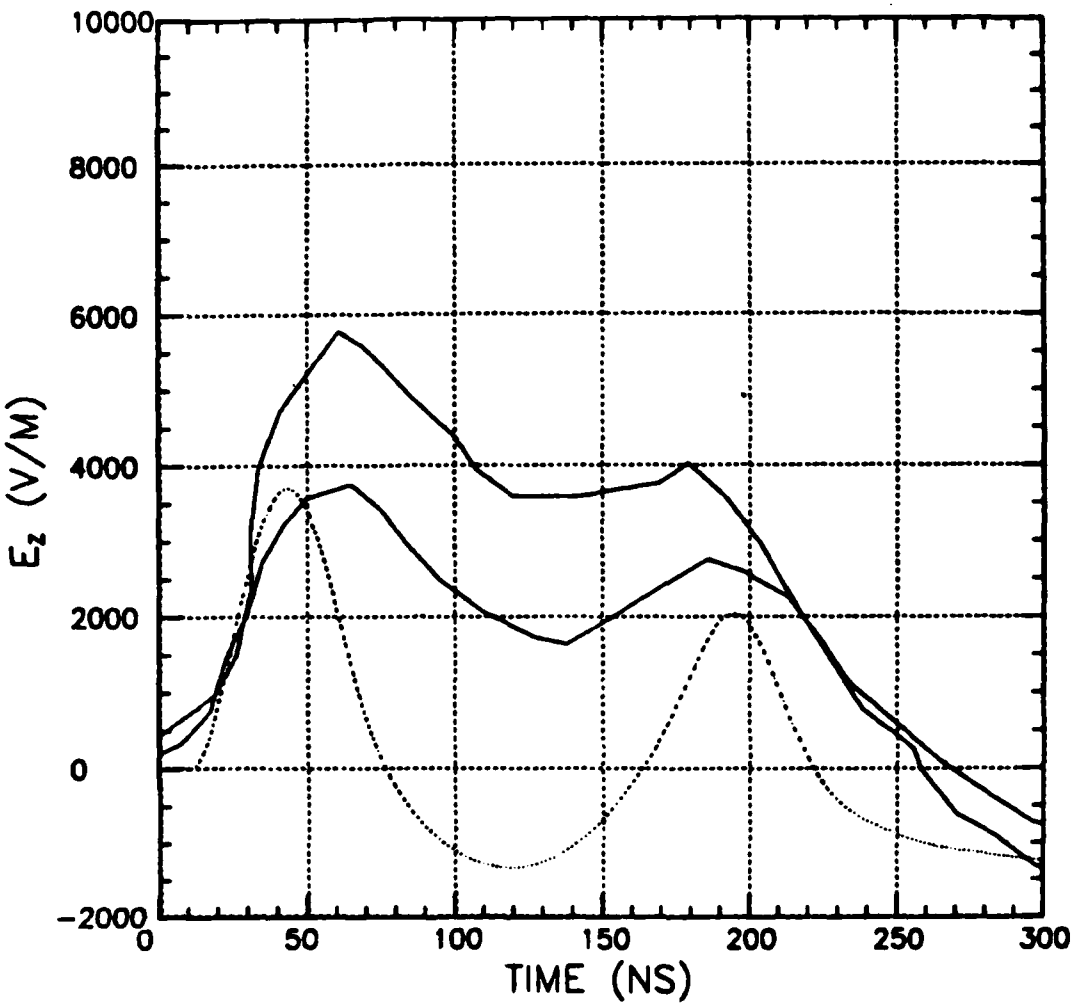

Figure 20. Comparison of measured electric fields in close to the AURORA source and AUR3D results (dotted line). The data are on the floor at y = 2 m and x = -0.5 m.

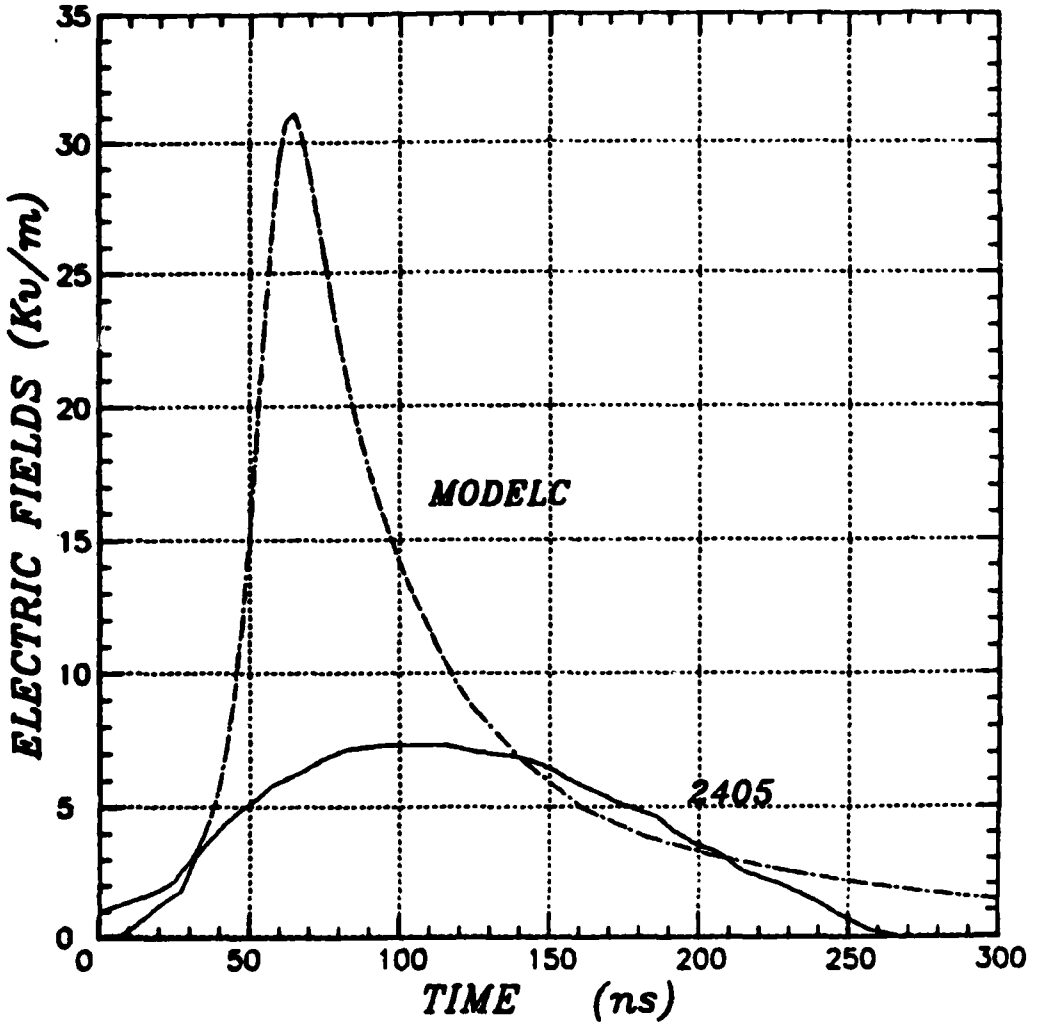

Figure 21. A comparison between the surface normal electric field measured in AURORA and the threat field computed with MODELC.

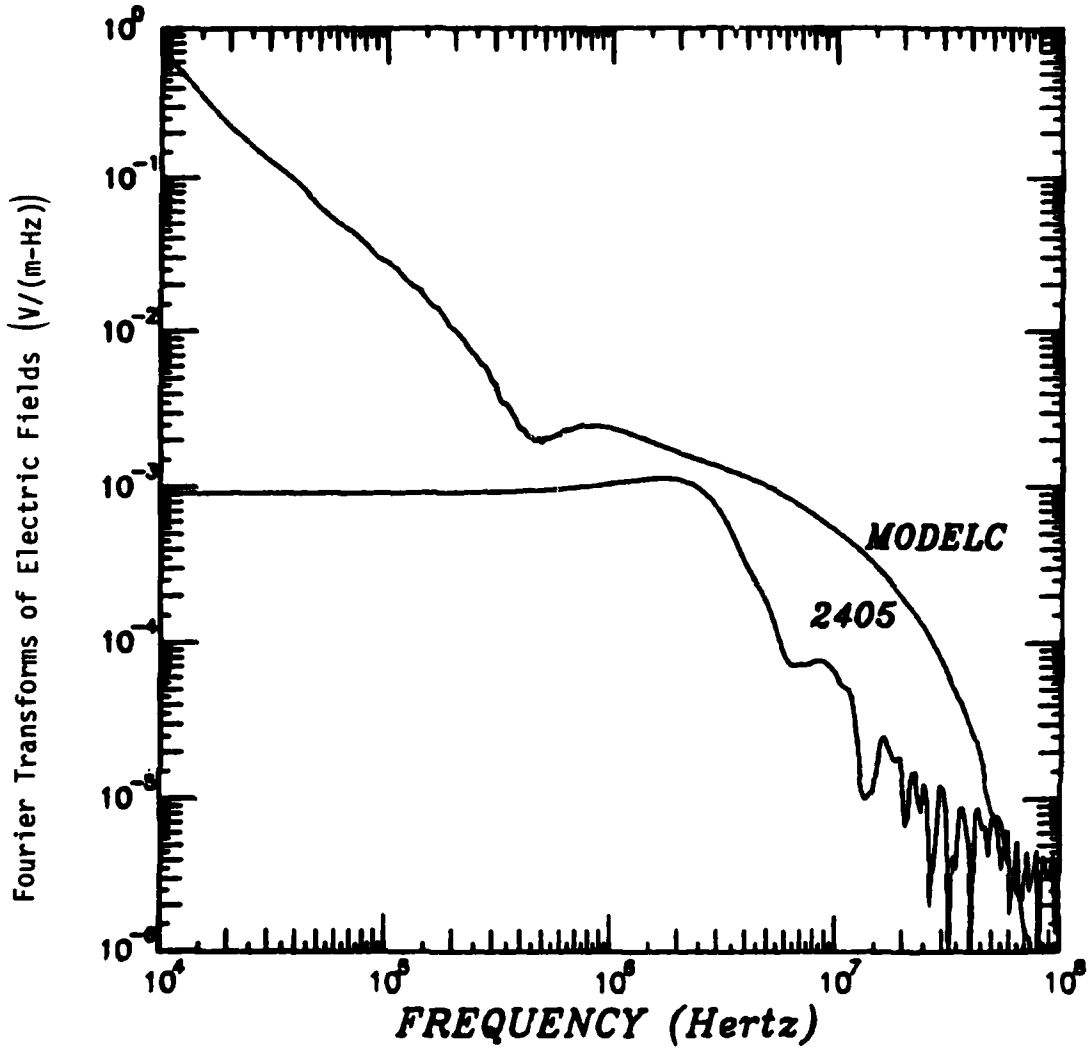

Figure 22. Fourier transforms of electric field wave forms shown in Figure 18.

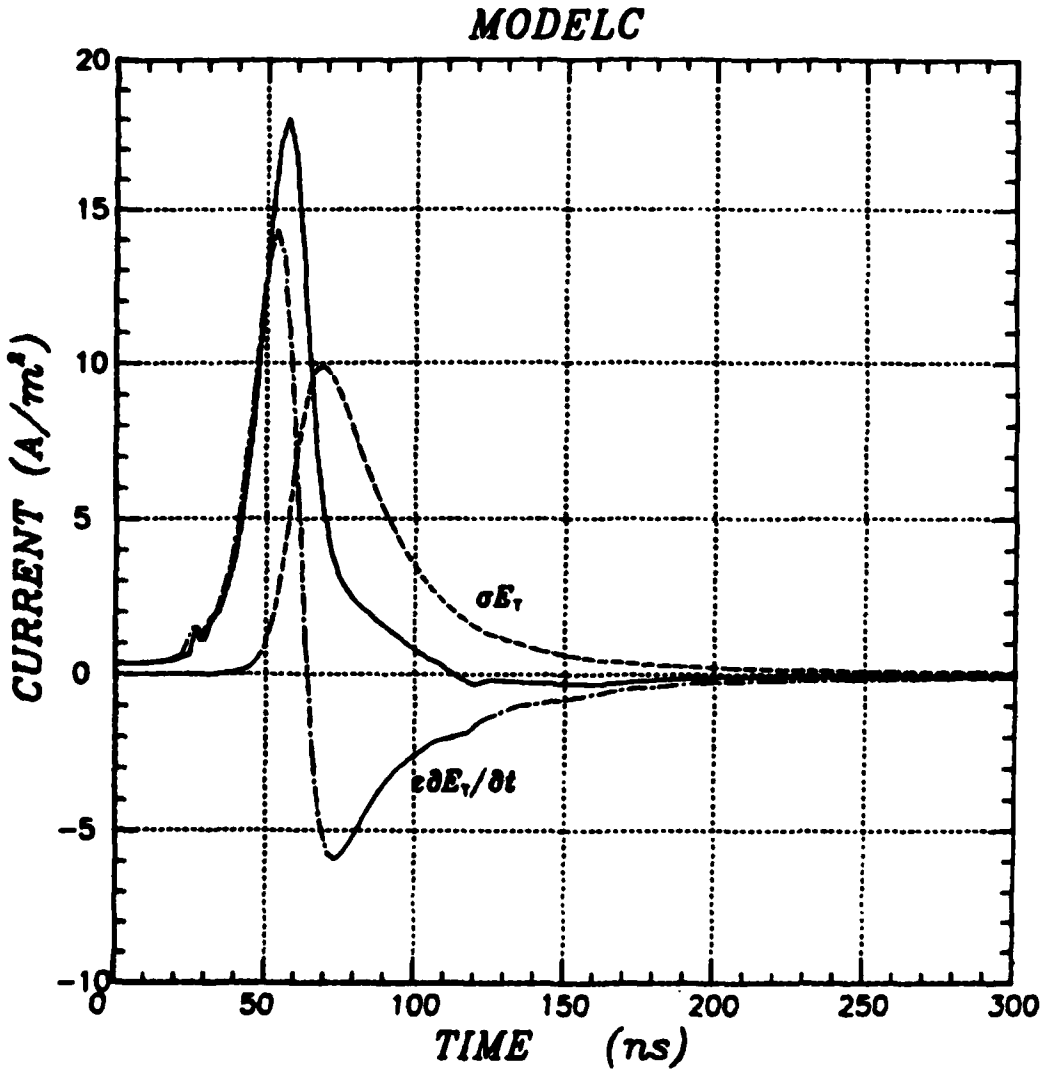

Figure 23. The threat conduction current (σE), displacement current (εδE/δt) and their sum (solid line).

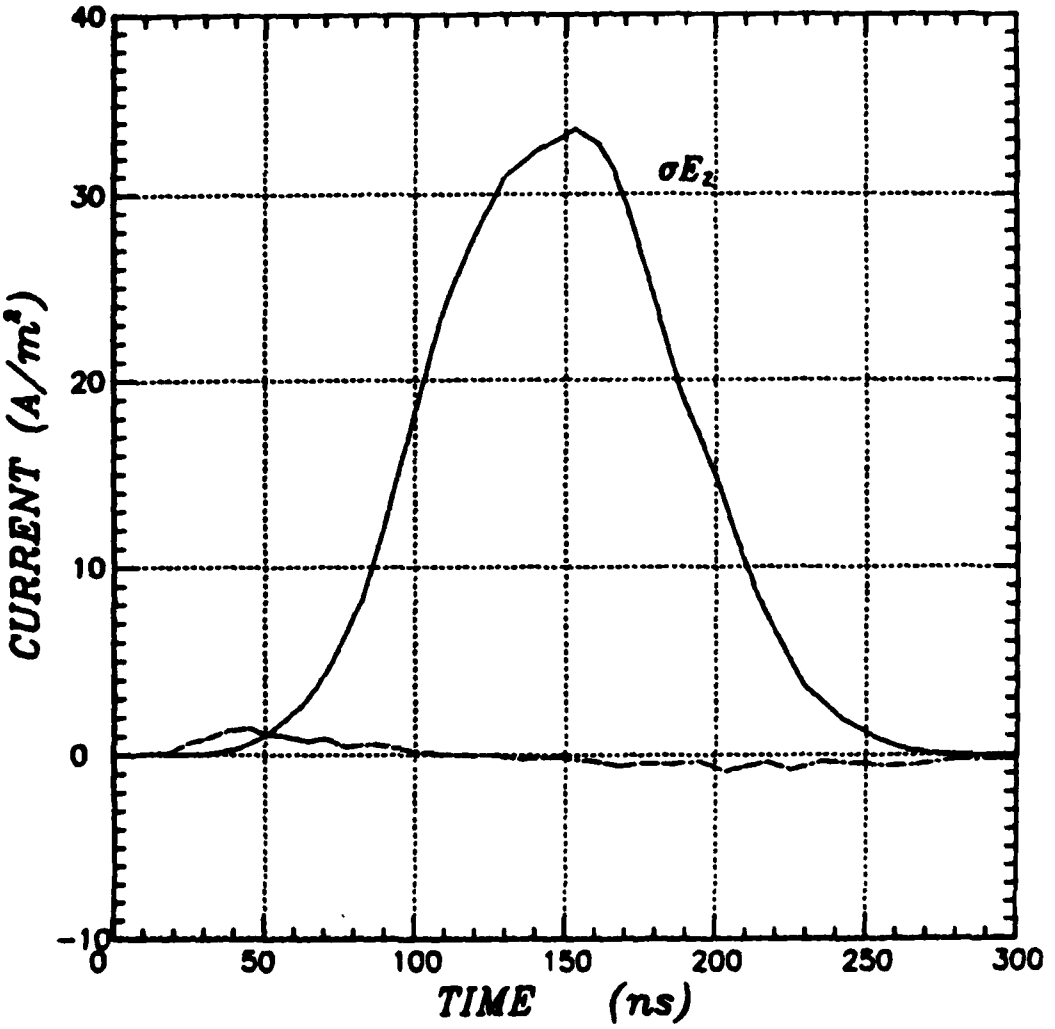

Figure 24. AURORA conduction current (σE), and displacement current (dashed line) on the floor at 4 m.

three times threat level. The reason for this is that we are in so close to the AURORA sources that the peak air conductivity is 4.5×10^{-3} mho/m or more than 10 times threat level.

If one were to go back 10 meters or so, where the air conductivity in AURORA peak at threat level, the electric fields would be smaller by a factor of 2 or 3 and the conduction current would be smaller by a factor of 30 or so. One can get threat level conduction currents in AURORA but only by greatly exceeding the threat level air conductivity.

CONCLUSIONS

As we have seen above, AURORA has many unique capabilities as a source region simulator. It can produce threat level Compton currents, magnetic fields, and conduction currents over moderate size volumes. We have also seen that its slow rise rate and limited size introduce important deviations from reality, particularly with regards to the electric field strength and its rise rate. The unmodified AURORA facility has many important uses but they tend to be fundamental in nature. The physics occurring in AURORA is basically the same physics that occurs in the threat environment. AURORA provides an opportunity to verify that we understand that physics and contributes to our confidence that we are computing the correct fields for the threat case. In many ways AURORA is more complicated than the threat environment and, in effect, provides an overtest of our predictive capability. The unmodified AURORA has also proven useful for verifying various coupling models, particularly to short antennas in the presence of ionizing radiation.[17]

The usefulness of the unmodified AURORA for testing the hardness of tactical Army systems is severely limited by the slow rise and low intensity of the electric field. Both the rise rate and peak intensity are about a factor of 10 smaller than threat level. For the past several years MRC and HDL have been studying ways to enhance the electric field in AURORA. The best method seems to be to use a low impedance transmission line. HDL has suggested a very promising design although there is some question as to how fast a rise time can be achieved with existing pulsers.

We feel that the unmodified AURORA should continue to be used to study the fundamental processes important in source region coupling - both tactical and strategic. For example, studies of the interaction between

energetic photons and material interfaces could help to increase our ability to predict coupling in the threat environments, especially where γ-thick objects such as tanks are concerned.

The lack of realistic electric fields in the AURORA test cell force us to conclude that an auxiliary electric field generation mechanism should be used in conjunction with the AURORA generated air conductivity and Compton current for actual hardness testing of tactical army systems such as radios. The fact that the air conductivity and Compton current rise more slowly than the threat compromises the realism of the simulation somewhat. However, the mere fact of their presence adds a dimension of realism not present in other simulators.

AURORA is not a panacea for all coupling simulations. First of all large systems can not be tested in AURORA because of size constraints. Smaller systems, with dimensions of a meter or so, are well suited for testing in AURORA. However, the lack of realism, in even a modified AURORA, requires that any experiments be supported with a strong analysis program to access the impact of the lack of simulation fidelity.

The cost of doing experiments in AURORA, compared with experiments in a non-ionizing environment, is very high. One should carefully consider how much testing can be done without using AURORA to characterize the particular system of concern. Analysis can then be used to predict the impact of air conductivity and predict the response in AURORA. One can then conduct a limited set of experiments in AURORA to verify the analytic models.

Thus we see a modified AURORA as playing a vital role in any tactical source region hardness verification program. But only as one of several tools one should use to characterize a particular system. By using the proper balance of the tools available to it, the Army can achieve a high level of confidence in its hardness program for a reasonable cost.

REFERENCES

1. Spohn, D.J. private communication.

2. Berberet, J., "EMP Hardness Levels for Army Tactical Equipment", abstracts of the DNA Source-Region EMP Technology and Systems Survivability Requirements Seminar, held at the Naval Postgraduate School, Monterey, California, 22-24 August 1978.

3. Glasstone, S., and P.J. Dolan, eds., The Effects of Nuclear Weapons, 3rd Edition, U.S. Government Printing Office, 1977.

4. Holst, D.W., The ARES for Stimulation of the Source Region Response in Tactical Systems, MRC-R-565, Mission Research Corporation, Santa Barbara, CA., April 1980.

5. Crevier, W.F., R.M. Hamilton, E. Pettus, and H. Price, User's Manual for the MODELC Code, AURORA EMP Memo 20, Mission Research Corporation, February 1980.

6. Longmire, C.L., "On the Electromagnetic Pulse Produced by Nuclear Explosions", IEEE Trans. on Antennas and Propagation, Vol. AP-26, No. 1, January 1978.

7. Longmire, C.L., General Considerations on Use of AURORA for Simulating EMP Coupling, AURORA EMP Memo 1, Mission Research Corporation, September 1975.

8. Crevier, W.F., Methods for Enhancing the Electric Fields in AURORA, AURORA EMP Memo 16, Mission Research Corporation, November 1978.

9. Crevier, W.F., Response of a Transmission Line in AURORA, Mission Research Corporation, October 1977.

10. Longmire, C.L., G. Merkel, and D.J. Spohn, "Simple Compton Current Density Measurement Technique," IEEE Trans. Nucl. Sci., NS-24, December 1977.

11. Baum, C.E., "Characteristics of the Moebius Striploop," Sensor and Simulation Note 7, December 1964.

12. Crevier, W.F., L.M. Anderson, G. Merkel, and D.J. Spohn, "Status of AURORA Environment Calculations", IEEETrans. Nucl. Sci, NS-25, December 1978.

13. Chadsey, W.L., H. Bloomberg, R. Ford, V. Pine, and D. Strickland, "Characteristics of the AURORA FXR Photon Radiation Field for SREMP Studies", IEEE Trans. Nucl. Sci., NS-24, December 1977.

14. Tumolillo, T.A., J.P. Wondra, J. Bombart, G. Merkel, and D.J. Spohn, "PRES-3D: A Computer Code for Self Consistent Solution of the Maxwell-Lorentz Three-Species Air-Chemistry Equations in Three Dimensions," IEEE Trans. Nucl. Sci., NS-24, December 1977.

15. Crevier, W.F., Surface Fields and Currents in the AURORA Test Cell, AURORA EMP Memo 10, Mission Research Corporation, January 1978.

16. Crevier, W.F., and D.W. Holst, A Modified Fluid Approach to SGEMP and IEMP, MRC-R-553, Mission Research Corporation, February 1980.

17. Manriquez, R., G. Merkel, W.D. Scharf, D. Spohn, "Electrically Short Monopole Antenna Response in an Ionizer Air Environment-Determination of Air Conductivity", IEEE Trans. Nucl. Sci., NS-26, December 1979.

DISTRIBUTION

ASSISTANT TO THE SECRETARY OF DEFENSE
ATOMIC ENERGY
ATTN MILITARY APPLICATIONS
ATTN EXECUTIVE ASSISTANT
WASHINGTON, DC 20301

DIRECTOR
DEFENSE COMMUNICATIONS AGENCY
ATTN CODE 312
ATTN CODE C313
ATTN CODE 430, PARKER
WASHINGTON, DC 20305

DEFENSE COMMUNICATIONS ENGINEER CENTER
1860 WIEHLE AVE
ATTN CODE R400
ATTN CODE R123, TECH LIB
RESTON, VA 22090

DIRECTOR
DEFENSE INTELLIGENCE AGENCY
ATTN DB 4C2, D. SPOHN
ATTN RTS-2A, TECH LIB
WASHINGTON, DC 20301

DIRECTOR
DEFENSE NUCLEAR AGENCY
ATTN NATA
ATTN TITL (4 COPIES)
ATTN RAEV
ATTN RAEE, G. BAKER (10 COPIES)
ATTN STNA
WASHINGTON, DC 20305

ADMINISTRATOR
DEFENSE TECHNICAL INFORMATION CENTER
ATTN DTIC-DDA (12 COPIES)
CAMERON STATION
ALEXANDRIA, VA 22314

JOINT CHIEFS OF STAFF
ATTN J-3 RM 2D874
WASHINGTON, DC 20301

NATIONAL COMMUNICATIONS SYSTEM
OFFICE OF THE MANAGER
DEPARTMENT OF DEFENSE
ATTN NCS-TS
WASHINGTON, DC 20305

DIRECTOR
NATIONAL SECURITY AGENCY
ATTN TDL
ATTN R-52, O. VAN GUNTEN
ATTN S-232, D. VINCENT
FT GEORGE G. MEADE, MD 20755

COMMANDER
BMD SYSTEMS COMMAND
DEPARTMENT OF THE ARMY
ATTN BMDSC-AOLIB
ATTN BMDSC-HLE, R. WEBB
PO BOX 1500
HUNTSVILLE, AL 35807

DIVISION ENGINEER
US ARMY ENGR. DIV. HUNTSVILLE
ATTN T. BOLT
PO BOX 1600, WEST STATION
HUNTSVILLE, AL 35807

DIRECTOR
US ARMY BALLISTIC RESEARCH LABS
ATTN DRDAR-BLB, W. VAN ANTWERP
ATTN DRDAR-BLE
ABERDEEN PROVING GROUND, MD 21005

COMMANDER
US ARMY COMMUNICATIONS COMMAND
ATTN CC-LOG-LEO
ATTN CC-OPS-WS, CONNELL
ATTN CC-OPS-PD
ATTN CC-OPS-OS
ATTN ATSI-CD-MD
FT HUACHUCA, AZ 85613

CHIEF
US ARMY COMMUNICATIONS SYS AGENCY
DEPARTMENT OF THE ARMY
ATTN CCM-AD-SV
ATTN CCM-RD-T
FT MONMOUTH, NJ 07703

COMMANDER
US ARMY NUCLEAR & CHEMICAL AGENCY
ATTN MONA-WE
ATTN DR. BERBERET
7500 BACKLICK ROAD
BUILDING 2073
SPRINGFIELD, VA 22150

COMMANDER
US ARMY TRAINING AND DOCTRINE COMMAND
ATTN ATCD-Z
FT MONROE, VA 23651

BMD CORP
ATTN CORPORATE LIBRARY
7915 JONES BRANCH DRIVE
MCLEAN, VA 22101

BENDIX CORP
COMMUNICATION DIVISION
ATTN DOCUMENT CONTROL
E JOPPA ROAD
BALTIMORE, MD 21204

DIKEWOOD CORPORATION
ATTN TECHNICAL LIBRARY
1613 UNIVERSITY BLVD, NE
ALBUQUERQUE, NM 87102

ELECTRO-MAGNETIC APPLICATIONS, INC.
ATTN D. MEREWETHER
PO BOX 8482
ALBUQUERQUE, NM 87198

GENERAL ELECTRIC CO.
SPACE DIVISION
VALLEY FORGE SPACE CENTER
ATTN J. ANDREWS
PO BOX 8555
PHILADELPHIA, PA 19101

GTE/SYLVANIA
ATTN J. KILLIAN
1 RESEARCH DRIVE
WESTBORO, MA 01581

HONEYWELL, INC.
AEROSPACE & DEFENSE GROUP
ATTN S. GRAFF
ATTN W. STEWART
13350 US HIGHWAY 19 SOUTH
CLEARWATER, FL 33516

IIT RESEARCH INSTITUTE
ELECTROMAG COMPATIBILITY ANAL CTR
ATTN ACOAT
N SEVERN
ANNAPOLIS, MD 21402

IIT RESEARCH INSTITUTE
ATTN I. MINDEL
10 W 35TH ST
CHICAGO, IL 60616

IRT CORP.
ATTN J. KNIGHTON
PO BOX 81087
SAN DIEGO, CA 92138

LUTECH, INC.
ATTN F. TESCHE
PO BOX 1263
BERKELEY, CA 94701

MARTIN MARIETTA CORP
ATTN M. GRIFFITH (2 COPIES)
ATTN J. CASALESE
ATTN B. BROULIK
PO BOX 5837
ORLANDO, FL 32855

MCDONNELL DOUGLAS CORP
ATTN S. SCHNEIDER
ATTN TECHNICAL LIBRARY SERVICES
5301 BOLSA AVE
HUNTINGTON BEACH, CA 92647

MISSION RESEARCH CORPORATION
ATTN J. RAYMOND
ATTN J. CHERVENAK
5434 RUFFIN ROAD
SAN DIEGO, CA 92123

MISSION RESEARCH CORP
ATTN W. CREVIER
ATTN C. LONGMIRE
ATTN EMP GROUP
PO DRAWER 719
SANTA BARBARA, CA 93102

MISSION RESEARCH CORPORATION
ATTN W. STARK
ATTN J. LUBELL
ATTN W. WARE
PO BOX 7816
COLORADO SPRINGS, CO 80933

RICHARD L. MONROE ASSOCIATES
1911 R STREET NW
SUITE 203
WASHINGTON, DC 20009

NORTHROP CORP.
ELECTRONIC DIVISION
ATTN LEW SMITH
ATTN RAD EFFECTS GRP
ATTN B. AHLPORT
2301 W 120TH ST
HAWTHORNE, CA 90250

R&D ASSOCIATES
ATTN DOCUMENT CONTROL
ATTN W. GRAHAM
ATTN C. MO
ATTN M. GROVER
PO BOX 9695
MARINA DEL REY, CA 90291

RAYTHEON CO
ATTN G. JOSHI
ATTN H. FLESCHER
HARTWELL ROAD
BEDFORD, MA 01730

ROCKWELL INTERNATIONAL
ATTN B-1 DIV TIC (BAOB)
PO BOX 92098
LOS ANGELES, CA 90009

SEA
MARINER SQUARE
ATTN W. HUTCHINSON
SUITE 127
1900 N. NORTHLAKE WAY
PO BOX 31819
SEATTLE, WA 98103

SRI INTERNATIONAL
ATTN E. VANCE
ATTN A. WHITSON
333 RAVENSWOOD AVE
MENLO PARK, CA 94025

TELEDYNE-BROWN ENGINEERING
ATTN D. GUICE
CUMMINGS RESEARCH PARK
HUNTSVILLE, AL 35807

TRW ELECTRONICS AND DEFENSE SYSTEMS GROUP
ATTN W. GARGARO
ATTN L. MAGNOLIA
ATTN R. PLEBUCH
ATTN C. ADAMS
ATTN H. HOLLOWAY
ATTN E. HORGAN
ATTN J. PENAR
ONE SPACE PARK
REDONDO BEACH, CA 90278

HARRY DIAMOND LABORATORIES
ATTN CO/TD/TSO/DIVISION DIRECTORS
ATTN RECORD COPY, 81200
ATTN HDL LIBRARY, 81100 (3 COPIES)
ATTN HDL LIBRARY, 81100 (WOODBRIDGE)
ATTN TECHNICAL REPORTS BRANCH, 81300
ATTN CHAIRMAN, EDITORIAL COMMITTEE
ATTN LEGAL OFFICE, 97000
ATTN BRANCH 20000
ATTN BRANCH 20240 (10 COPIES)
ATTN BRANCH 21100
ATTN BRANCH 21200
ATTN BRANCH 21300 (10 COPIES)
ATTN BRANCH 21400
ATTN BRANCH 21500
ATTN BRANCH 21000
ATTN BRANCH 22000
ATTN BRANCH 22300 (2 COPIES)
2800 POWDER MILL RD
ADELPHI, MD 20783